ARMY RESEARCH LABORATORY

Detection of Energetic Materials and Explosive Residues With Laser-Induced Breakdown Spectroscopy: II. Stand-off Measurements

by Jennifer L. Gottfried, Frank C. De Lucia Jr., Chase A. Munson, Christopher Ford, and Andrzej W. Miziolek

ARL-TR-4241 **September 2007**

NOTICES

Disclaimers

Army Research Laboratory
Aberdeen Proving Ground, MD 21005-5066

ARL-TR-4241 **September 2007**

Detection of Energetic Materials and Explosive Residues With Laser-Induced Breakdown Spectroscopy: II. Stand-off Measurements

Jennifer L. Gottfried, Frank C. De Lucia Jr., Chase A. Munson, Christopher Ford, and Andrzej W. Miziolek
Weapons and Materials Research Directorate, ARL

REPORT DOCUMENTATION PAGE

Form Approved
OMB No. 0704-0188

1. REPORT DATE *(DD-MM-YYYY)*	2. REPORT TYPE	3. DATES COVERED (From - To)
September 2007	Final	November 2005–April 2007

4. TITLE AND SUBTITLE
Detection of Energetic Materials and Explosive Residues With Laser-Induced Breakdown Spectroscopy: II. Stand-off Measurements

5a. CONTRACT NUMBER

5b. GRANT NUMBER

5c. PROGRAM ELEMENT NUMBER

6. AUTHOR(S)
Jennifer L. Gottfried, Frank C. De Lucia Jr., Chase A. Munson, Christopher Ford, and Andrzej W. Miziolek

5d. PROJECT NUMBER
622618H8049

5e. TASK NUMBER

5f. WORK UNIT NUMBER

7. PERFORMING ORGANIZATION NAME(S) AND ADDRESS(ES)
U.S. Army Research Laboratory
ATTN: AMSRD-ARL-WM-BD
Aberdeen Proving Ground, MD 21005-5066

8. PERFORMING ORGANIZATION REPORT NUMBER
ARL-TR-4241

9. SPONSORING/MONITORING AGENCY NAME(S) AND ADDRESS(ES)

10. SPONSOR/MONITOR'S ACRONYM(S)

11. SPONSOR/MONITOR'S REPORT NUMBER(S)

12. DISTRIBUTION/AVAILABILITY STATEMENT
Approved for public release; distribution is unlimited.

13. SUPPLEMENTARY NOTES

14. ABSTRACT
We have developed a double pulse stand-off laser-induced breakdown spectroscopy (LIBS) system capable of detecting explosive residues as far as 50 m. As described in an earlier report (ARL-TR-4240), the use of a double pulse laser improves the sensitivity and selectivity of LIBS for the detection of energetic materials. This report discusses the extension of these studies to stand-off distances. The efficacy of chemometric techniques such as linear correlation, principal components analysis, and partial least squares discriminant analysis for the identification of explosive residues is also discussed. We have shown that despite the typical characterization of LIBS as an elemental technique, the relative elemental intensities in the LIBS spectra are representative of the stoichiometry of the parent molecules and can be used to discriminate materials containing the same elements.

15. SUBJECT TERMS
explosive detection, LIBS, standoff

16. SECURITY CLASSIFICATION OF:			17. LIMITATION OF ABSTRACT	18. NUMBER OF PAGES	19a. NAME OF RESPONSIBLE PERSON
a. REPORT	b. ABSTRACT	c. THIS PAGE			Jennifer L. Gottfried
UNCLASSIFIED	UNCLASSIFIED	UNCLASSIFIED	UL	48	19b. TELEPHONE NUMBER (*Include area code*) 410-306-0884

Standard Form 298 (Rev. 8/98)
Prescribed by ANSI Std. Z39.18

Contents

List of Figures

List of Tables

1. Introduction

The detection and discrimination of energetic materials with the use of laser-induced breakdown spectroscopy (LIBS) has been demonstrated in an earlier report (*1*). One of the main advantages of LIBS is the capability for remote sensing. Stand-off detection of explosives with LIBS offers real-time results while a safe distance is maintained for the operator. In December 2004, a group led by the U.S. Army Research Laboratory (ARL) successfully tested stand-off LIBS technology using a single-pulse laser source for the detection of residue amounts of explosives on a vehicle at a distance of 30 m at Yuma Proving Ground (YPG), Arizona (*2*). After the successful YPG stand-off tests, three stand-off sensors based on LIBS (ST-LIBS) were developed by ARL in conjunction with its partners, Applied Photonics, Ltd, and Ocean Optics, Inc.

With each generation, significant design improvements have been made, including the incorporation of a double pulse laser and full broadband (ultraviolet [UV]-visible [VIS]-near infrared [NIR]) detection. As discussed in reference (*1*), double pulse LIBS is extremely important for the detection of energetic materials. Since the identification of explosives depends on determining the abundance of nitrogen and oxygen relative to carbon and hydrogen (which is higher in energetic materials compared to non-energetic materials, see table 1), the ability of double pulse LIBS to reduce the amount of air entrained in the plasma event is essential. In the context of stand-off LIBS, the increase in sensitivity because of double pulsing results in a longer effective stand-off detection range. Section 2 describes the design and capabilities of the ST-LIBS systems. We then present results demonstrating the importance of double pulse LIBS for stand-off detection. Finally, we discuss chemometric techniques for identifying explosive residues and explosive-containing mixtures as far as 50 m using the ST-LIBS system.

Table 1. Molecular formulas for common explosives and potential interferents.

Explosive	**Formula**	**Potential Interferent**	**Formula**
RDX	$C_3H_6N_6O_6$	Polyurethane	$C_{17}H_{15}O_4N_2$
TNT	$C_7H_5N_3O_6$	Methyl-2-cyanoacrylate	$C_5H_5O_2N$
PETN	$C_5H_8N_4O_{12}$	Diesel Fuel	$C_{10}H_{22}$-$C_{15}H_{32}$
HMX	$C_4H_8N_8O_8$	Oils (fatty acids)	$CH_3(CH_2)_2COOH$, $CH_3(CH_2)_{18}COOH$

2. Experimental

2.1 Stand-off LIBS Instrumentation

The first generation ST-LIBS system (Gen 1) incorporates a Big Sky* CFR400-PIV† double pulse laser (1064 nm, 2 Hz, 250 mJ/pulse, <10 ns pulse width). The Big Sky lasers were chosen for their small footprint and rugged design. A commercially available 8-in Schmidt-Cassegrain telescope by Meade (LX200GPS) is used to collect the LIBS emission along the same path traversed by the laser ablation beam. The combined double-laser pulse is directed along the axis of the telescope by an articulating arm, thus enabling a full range of motion on the telescope for ease in targeting the sample. A diode laser (632 nm) coincident with the IR laser illuminates the target spot. The infrared double pulse beam is expanded with a simple two-lens system and is focused down range by a 3-in positive lens (f = 475 mm). Plasma light collected by the telescope is focused into a fiber optic and sent to a gated charge coupled device (CCD) spectrometer (500 to 900 nm) developed by Ocean Optics, Inc. The Ocean Optics software is used to fire the lasers (single shot) and collect the spectral data. A digital camera and wireless range finder enable remote viewing and measurement of the distance to the target.

Although we were able to collect spectra of metals and explosive residues on metals at 20 m with the Gen 1 system, we found that the poor beam quality of the lasers in the far field resulted in a weaker plasma that made obtaining LIBS spectra of organic materials extremely challenging. For the second generation (Gen 2) system, therefore, Quantel Brilliant Twins lasers (1064 nm, 10 Hz, 335 mJ/pulse, 5 ns pulse width) were chosen as the double pulse laser source and were found to provide superior beam quality ($M^2 < 2$) and power at 20+ meters. As with the Gen 1 system, the two laser beams are combined before entering the articulating arm. A 14-in Meade telescope (LX200GPS) was fitted with UV-coated optics to provide greater light-gathering power compared to Gen 1 and full broadband (UV-VIS-NIR) capability. A three-channel gated CCD spectrometer developed by Ocean Optics provides high light-throughput and sensitivity from 190 to 840 nm. The entire system is mounted on a wheeled cart and is easily transportable. Figure 1 shows a photograph of the Gen 2 system. We have determined the optimal timing parameters for this system (with the Ocean Optics spectrometer) as having a delay time t_{delay}=2 µs, integration time gate t_{int}=100 µs, and interpulse separation Δt=3 µs.

A third generation ST-LIBS system (Gen 3) has been designed to address the issue of eye safety. A single Quantel Brilliant B laser (1064 nm, 10 Hz, 850 mJ, 6 ns pulse width) is shifted to 1.54 µm with the use of a CH_4/Ar-filled Raman cell developed by the National Center for

*Big Sky Laser Technologies is a subsidiary of the Quantel Group (France).
†Not an acronym.

Figure 1. Photograph of the Gen 2 double pulse ST-LIBS system developed by ARL in collaboration with Applied Photonics, Ltd, and Ocean Optics, Inc.

Atmospheric Research (NCAR). As with the Gen 2 system, a modified 14-in Meade telescope is used to collect the light emitted from the laser-induced plasma. Testing of this system is under way and the results will be reported in a subsequent paper.

2.2 Materials and Methods

With the Gen 2 system, spectra of each of the following samples were acquired at 20 m. For residue detection, ~4 to 5 mg of the powdered forms of pure explosives (cyclotrimethylene-trinitramine [RDX], 2,4,6-trinitrotoluene [TNT], or Comp-B [63% RDX, 36% TNT, 1% wax]) were dissolved in ~3 mL of acetone and applied to a heavy duty aluminum (Al) foil substrate via a 10-µL syringe. The Al foil samples were used straight from the roll without additional cleaning. The interferent Arizona road dust (standard reference material) was provided by Battelle and applied to the Al foil in a very thin layer.

A commercial lubricant (WD-40[*]) was used for the oil interferent. A small amount was sprayed on the Al substrate and then wiped almost completely off with a clean room cloth. We applied fingerprint residue by repeatedly handling the surface of the Al with clean hands (depositing oil from the surface of the skin in a fingerprint pattern). The lid from a food container was used for the white Type V (polypropylene $(C_3H_6)_x$) plastic sample. The anthrax surrogate *Bacillus subtilis var. niger* (commonly known as *Bacillus globigii*, or BG) and mold sample *Alternia*

[*]WD-40 is a registered trademark of the WD-40 Company.

alternata (AA) were provided by Battelle. Residue samples of the biomaterials (biological interferents) were prepared in an analogous manner to the explosive residue (~4 to 5 mg dissolved in 3 mL of acetone).

RDX and dust mixtures (50% weight by weight) were prepared with two methods. For the first method, 2.5 mg of RDX and 2.5 mg of Arizona dust were dissolved in 3 mL of acetone. The solution was thoroughly mixed and quickly applied to the Al foil via a 10-μL syringe. Although this method provides a homogeneous mixture, it does not represent "real-world" conditions, so a second method was employed. A thin layer of Arizona dust was applied to the Al foil, and several milligrams of RDX powder were crushed onto the surface (~60 cm^2), thus creating an inhomogeneous mixture. We similarly prepared an oil and dust mixture by smearing a clean room cloth soaked with oil on a thin layer of dust. Spectra of explosive residue, interferent, and mixture samples were also acquired at 30 m and 50 m, as described in section 3.4.

Linear correlation analysis of the total ST-LIBS spectra (190 to 840 nm) and specific peak intensities and ratios was performed with the data analysis feature of Excel[*]. Principal components analysis (PCA), soft independent method of class analogy (SIMCA), and partial least squares discriminant analysis (PLS-DA) models were generated with the use of the PLS_Toolbox version 3.5 (Eigenvector Technologies, Inc.) running under MATLAB[†] version 7.0. The data were auto-scaled before the models were built.

3. Results and Discussion

3.1 Advantages of Double Pulse Stand-off LIBS

At 20 m, the ST-LIBS double pulse spectra show a dramatic improvement over single laser pulse spectra with the same total energy. With only one of the Quantel lasers on the Gen 2 system (275 mJ), 20 spectra each of Al foil and RDX residue on Al were acquired. The energies of both lasers were then reduced to give a total energy of 275 mJ (approximately 138 mJ/pulse) and double pulse spectra of the same samples were recorded (with Δt=3 μs). The averaged Al spectra are shown in figure 2 along with single- and double pulse spectra of Al measured in the laboratory for comparison. The laboratory spectra were acquired with an intensified CCD (ICCD) spectrometer that used 320 mJ total pulse energy from one or two (with Δt=2 μs) Continuum Surelite[‡] lasers. At stand-off distances, the Al lines are enhanced by a factor of at least 20 with double pulsing, so that the strongest Al I lines at 394 and 396 nm saturate the detector and many weaker Al I lines appear. A number of strong Al II lines that appear in both

[*]Excel is a trademark of Microsoft Corporation.
[†]MATLAB is a registered trademark of The MathWorks.
[‡]Surelite is a trademark of Continuum; Continuum is a registered trademark.

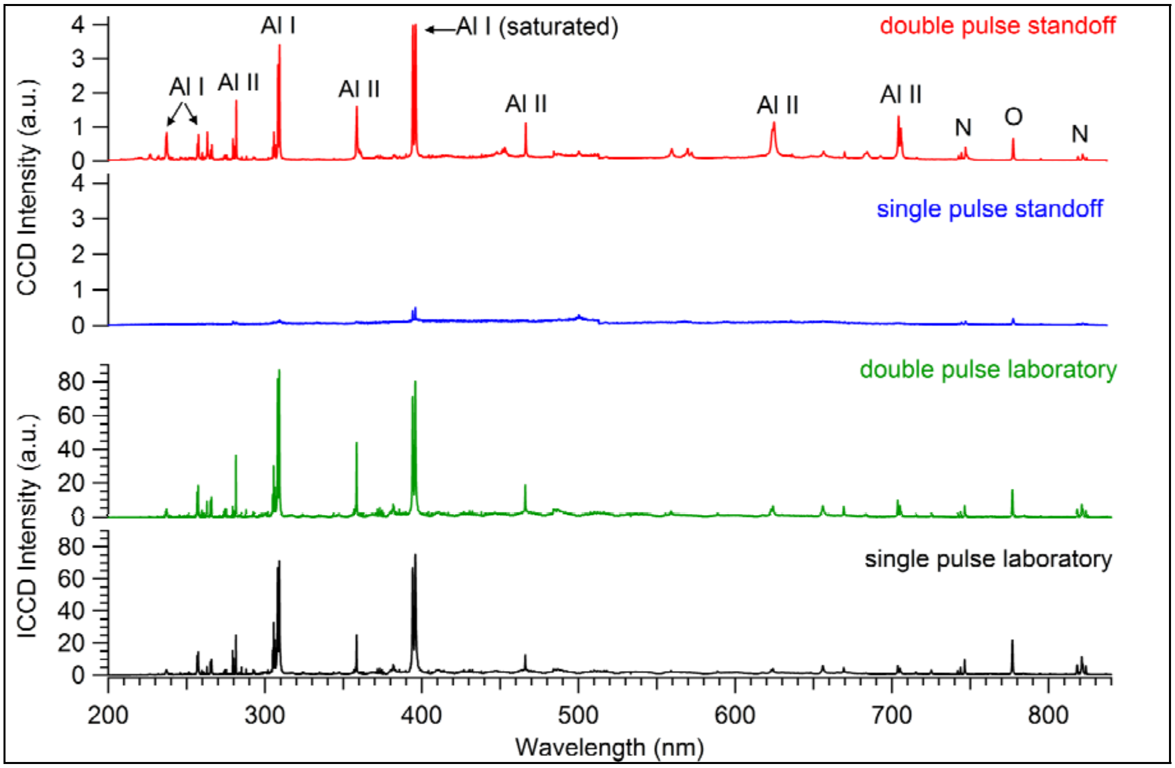

Note: a.u. = arbitrary units.

Figure 2. LIBS spectra (20 shots averaged) of Al (from top to bottom): at 20 m with a double pulse laser (275 mJ total energy, Δt=3 µs, CCD spectrometer); at 20 m with a single 275 mJ pulse; at close contact with a double pulse laser (320 mJ total energy, Δt=2 µs, ICCD spectrometer); and at close contact with a single 320-mJ pulse. (Strong emission lines from the Al sample [with residual air entrainment] are labeled for reference.)

the single- and double pulse laboratory spectra appear only in the double pulse ST-LIBS spectra. The increase in signal with double pulsing is not as dramatic for the laboratory system, which has a higher pulse energy density because of the smaller laser spot size at the target and higher power lasers. The stand-off lasers are not as tightly focused at 20 m as the laboratory system, which could explain the different behavior between the two systems.

For explosive residue detection, the fact that double pulse LIBS reduces the amount of atmospheric oxygen and nitrogen entrained in the (second) laser-induced plasma is even more important than the signal enhancement (*1*). Peak intensities of Al I (309 nm), Al II (622-624 nm) and O (777 nm) from ST-LIBS spectra of Al as a function of Δt are shown in figure 3. Spectra of the Al sample were recorded with a fixed delay time (t_{delay}=2 µs) and integration time gate (t_{int}=100 µs) with a single laser pulse of 275 mJ (Δt=0 µs) or two laser pulses with a total energy of 275 mJ separated in time by Δt. The increase in signal intensity with double pulsing is readily apparent, but the O/Al I ratio shows that at Δt=3 µs the air entrainment is minimized. Because the Al surface is not perfectly clean and the elimination of atmosphere oxygen is incomplete, the O/Al I ratio never reaches exactly zero.

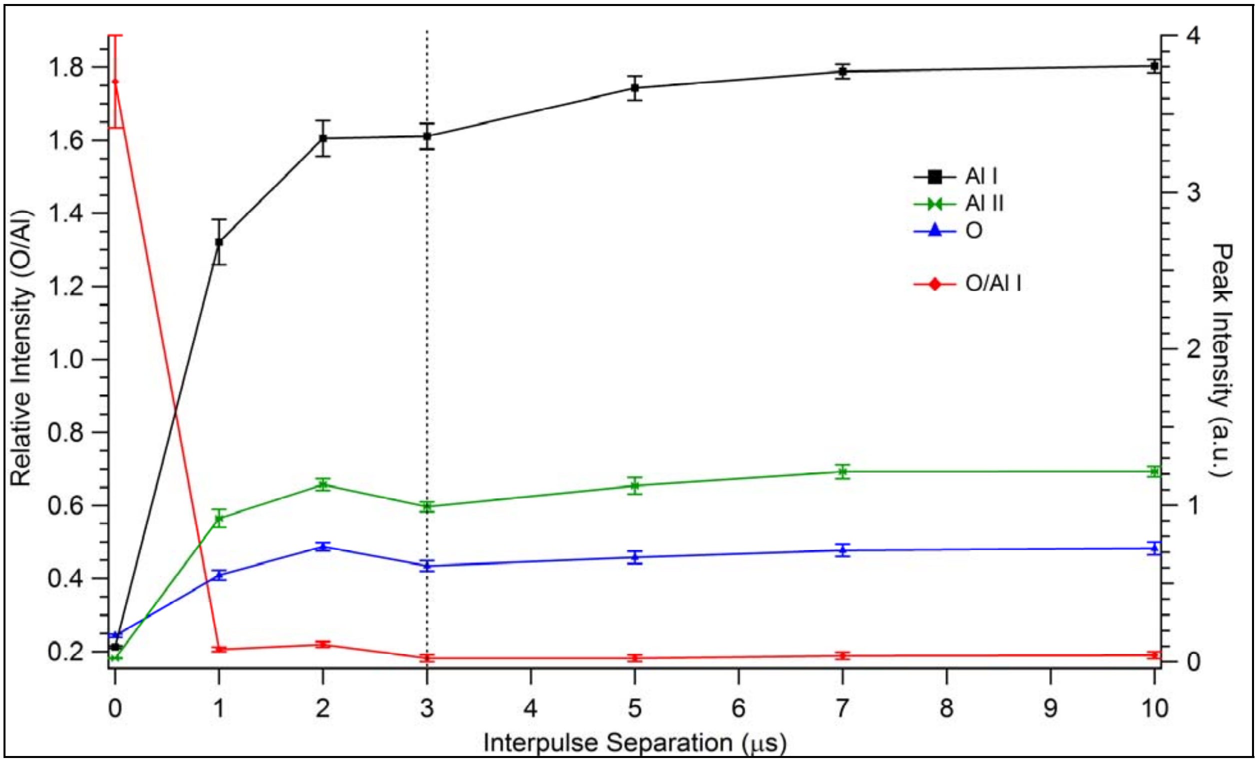

Figure 3. Peak intensities of Al I (309 nm), Al II (624 nm), and O (777 nm) and the relative O/Al I intensity are graphed as a function of interpulse separation Δt. (Error bars representing $\pm\sigma$ are given. Spectra of the Al sample at 20 m were recorded with a fixed delay time [t_{delay}=2 μs] and integration time gate [t_{int}=100 μs]. Δt=0 μs corresponds to a single laser pulse of 275 mJ, while Δt>0 μs corresponds to two laser pulses with a total energy of 275 mJ separated in time by Δt. The dashed line at Δt=3 μs represents the optimal interpulse separation time, as determined by the minimum value of O/Al I [i.e., minimal air entrainment].)

Figure 4 compares the O/N ratio for Al and RDX residue as a function of interpulse separation. For single pulses (Δt=0 μs), the average values of O/N for Al and RDX overlap (within one standard deviation). Such overlap because of contributions from atmospheric oxygen and nitrogen severely hampers the ability to discriminate between energetic and non-energetic materials (*1*). The greatest differential between the O/N ratios of Al and RDX occurs at Δt=3 μs. At Δt=3 μs the higher O/N ratio is indicative of the RDX (which has a stoichiometric oxygen-to-nitrogen ratio of 1:1) while the O/N ratio for Al reflects contributions from the atmosphere (~20% oxygen and ~80% nitrogen, or 1:4). Based on the results in figures 3 and 4, the optimal interpulse separation for the detection of explosive residues on Al substrates with our system is Δt =3 μs.

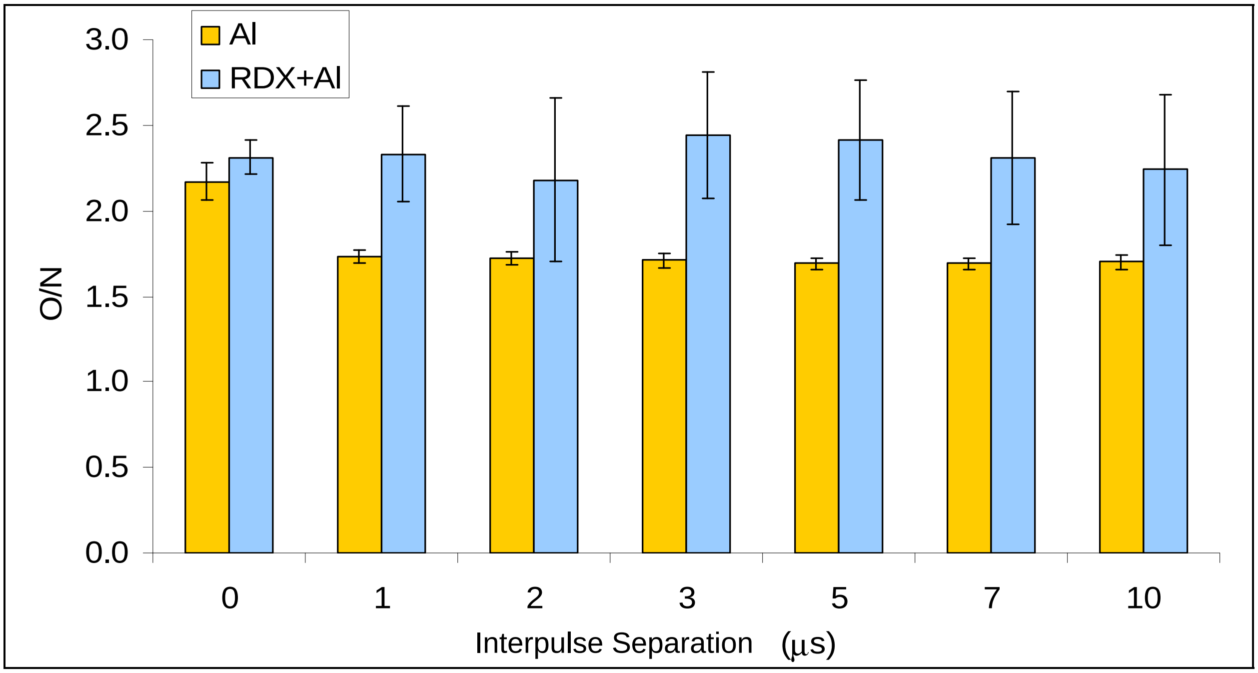

Figure 4. Comparison of the O/N ratio as a function of interpulse separation Δ*t* for Al and RDX residue on Al (spectra acquired at 20 m). (For single pulses [Δ*t*=0 μs], the average values of O/N for Al and RDX overlap [within one standard deviation]. The maximum separation between the O/N ratios occurs at Δ*t*=3 μs, indicating minimal air entrainment.)

Figure 5 compares the single- vs. double pulse LIBS spectra of RDX residue with the laboratory system (with a Catalina Echelle/Andor* i-Star ICCD spectrometer) described in reference (*1*) and the ST-LIBS system (with a three-channel gated CCD spectrometer by Ocean Optics). Although the close-contact double pulse spectrum of RDX residue shows some signal enhancement over the close-contact single-pulse spectrum, the increase in emission intensity is not as dramatic as that seen for the stand-off double pulse spectrum (compared to the single-pulse stand-off spectrum). Although the signal intensities of the H (656 nm), N (742, 744, and 747 nm), and O (777 nm) lines only increase by a factor of 2 or 3 with double pulsing on the stand-off system, the much weaker C line (247 nm) consistently appears only in the double pulse spectra. Interestingly, the increase in oxygen because of the presence of RDX results in the appearance of AlO molecular peaks around 500 nm in the ST-LIBS spectra. These peaks do not appear in the close-contact spectra, thus suggesting that the stand-off system produces a lower temperature plasma.

Figure 6 shows the relative O/C, O/N, and N/C ratios for RDX residue spectra acquired with the ST-LIBS system at 20 m as a function of interpulse separation (averaged values for 20 spectra with relative standard deviations 15 to 30%). The O/C and N/C ratios are minimized at Δ*t*=3 μs, while O/N reaches a maximum. This once again confirms that for this application the air entrained into the plasma is minimized at the optimal interpulse separation of Δ*t*=3 μs.

---

*Andor is a trademark of Andor Technology.

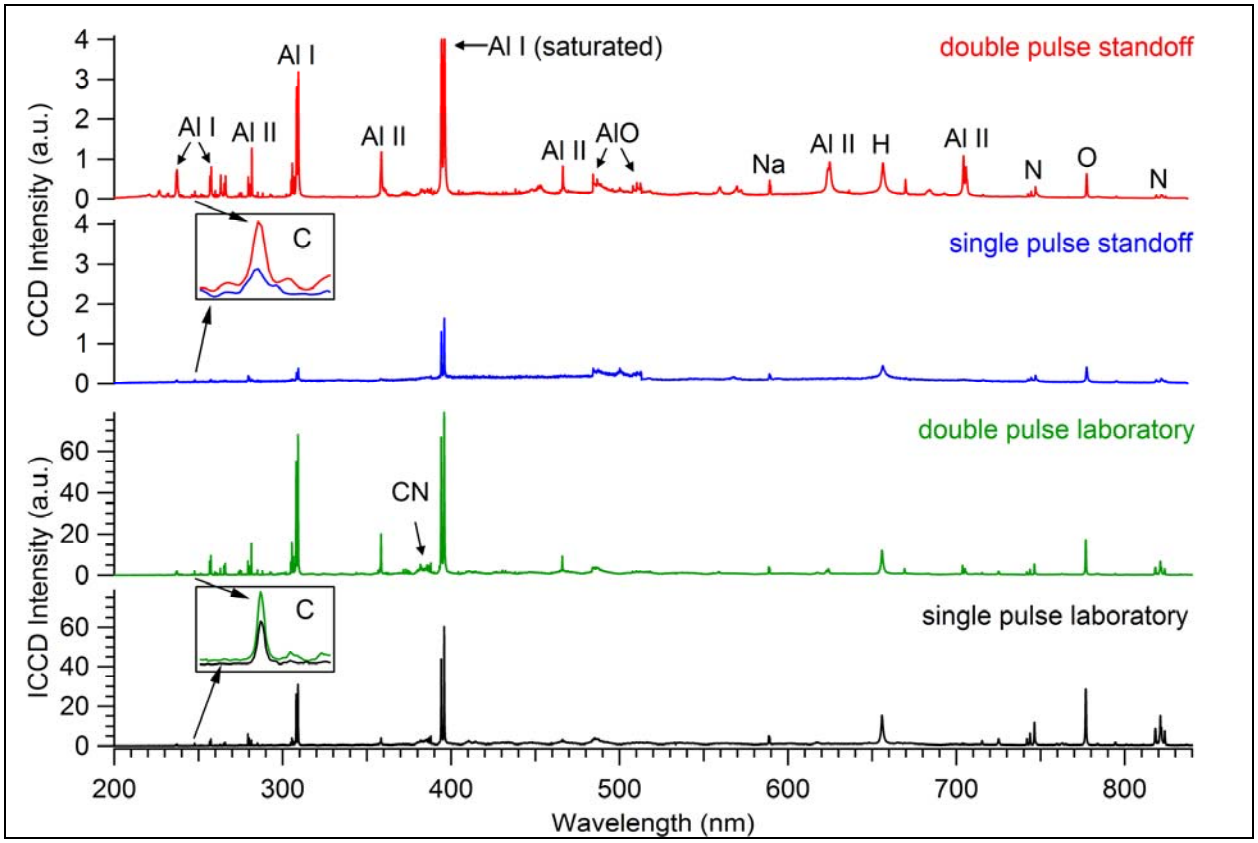

Figure 5. LIBS spectra (20 shots averaged) of RDX residue on Al (from top to bottom): at 20 m with a double pulse laser (275 mJ total energy, Δt=3 μs, CCD spectrometer); at 20 m with a single 275 mJ pulse; at close contact with a double pulse laser (320 mJ total energy, Δt=2 μs, ICCD spectrometer); and at close contact with a single 320-mJ pulse. (Strong emission lines are labeled for reference and the C line at 247 nm is inset and magnified on a 2-nm scale.)

3.2 Explosive Residue and Interferent Spectra at 20 m

After the optimal timing (t_{delay}, Δ*t*, and t_{int}) for the ST-LIBS system was determined, spectra of a number of explosive samples and interferents were acquired at 20 m with full laser power (~550 mJ total energy, Δt=3 μs). Figure 7 shows the single-shot spectra of an RDX pellet, solid Comp-B, and a white polypropylene (Type V) plastic. All three samples contain C (247 nm), CN (388 nm), and H (656 nm), but the explosive samples contain significantly more N (747 nm) and O (777 nm), as expected. Titanium lines present in the plastic (around 500 nm) are indicative of white pigmentation. These examples demonstrate the ability of the second generation ST-LIBS system to detect pure organic materials at 20 m.

Single-shot LIBS spectra of RDX, TNT, and Comp-B residues prepared on an Al substrate are shown in figure 8. In addition to the Al I-II and AlO emission caused by ablation of the Al substrate, the explosive residue spectra contain C, CN, Ca, C_2, Na, H, N, K, and O lines (the Ca and C_2 peaks are very weak in most spectra). Calcium, sodium and potassium were the only

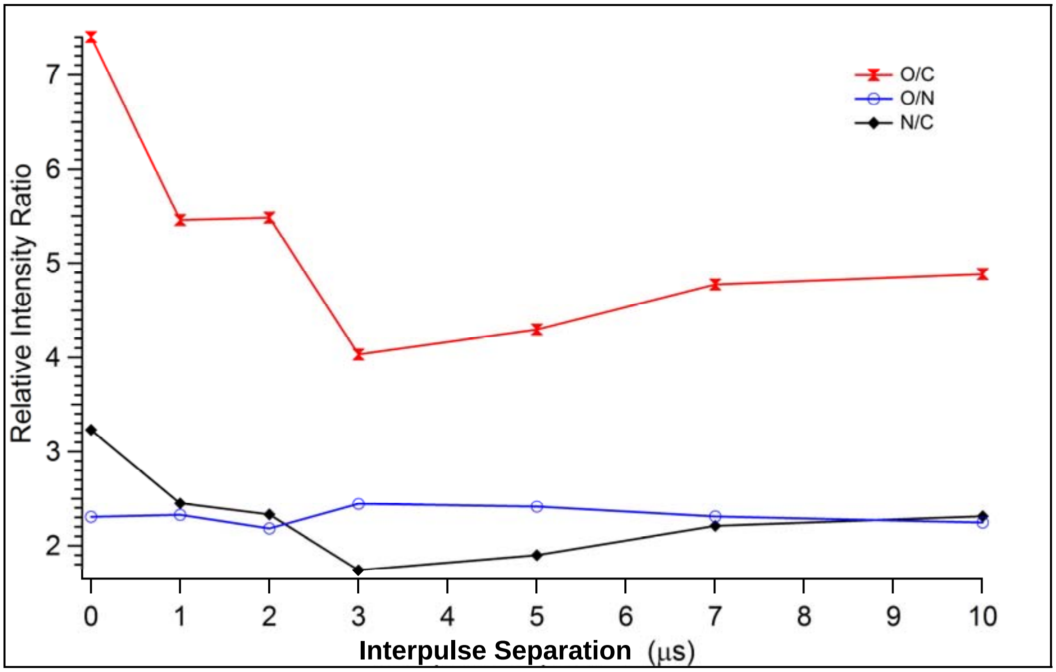

Figure 6. Relative intensities (O/C, O/N, N/C) vs. interpulse separation for an RDX residue sample spectrum acquired at 20 m. (Values are averaged over 20 spectra; for clarity, the error bars [15 to 30%] are not shown [but follow the same trends shown in the figure]. The optimal delay between pulses occurs at Δt=3 μs, where the O/C and N/C ratios are minimized and the O/N ratio is maximized, indicating minimal air entrainment.)

impurities observed in the explosives spectra. Figure 9 shows single-shot LIBS spectra of the biological, inorganic, and organic interferents used in these studies (the intensity scales for the different samples are identical to those in figure 8 but have been omitted for clarity). Differences in the broadband spectra shown in figure 9 are difficult to detect without the aid of chemometric techniques, since many of the substances contain the same elements. Because the spectra were acquired with a double pulse laser, which minimizes background signals from the air, key ratios of the elements in explosives can be used to discriminate among the different samples. Section 3.3 discusses the effectiveness of different techniques for explosives discrimination via LIBS spectra.

3.3 Advanced Chemometric Analysis for Explosives Discrimination

Although the double pulse ST-LIBS results discussed in the previous section demonstrate the detection of explosive residues at stand-off distances with LIBS, the discrimination of explosive and non-explosive residues requires further analysis. The ideal technique would provide low false negative rates for the detection of explosive samples and low false positive rates for non-explosive samples. In addition, the technique should be capable of (a) correctly classifying unknown samples not incorporated in the model as explosive or non-explosive and (b)

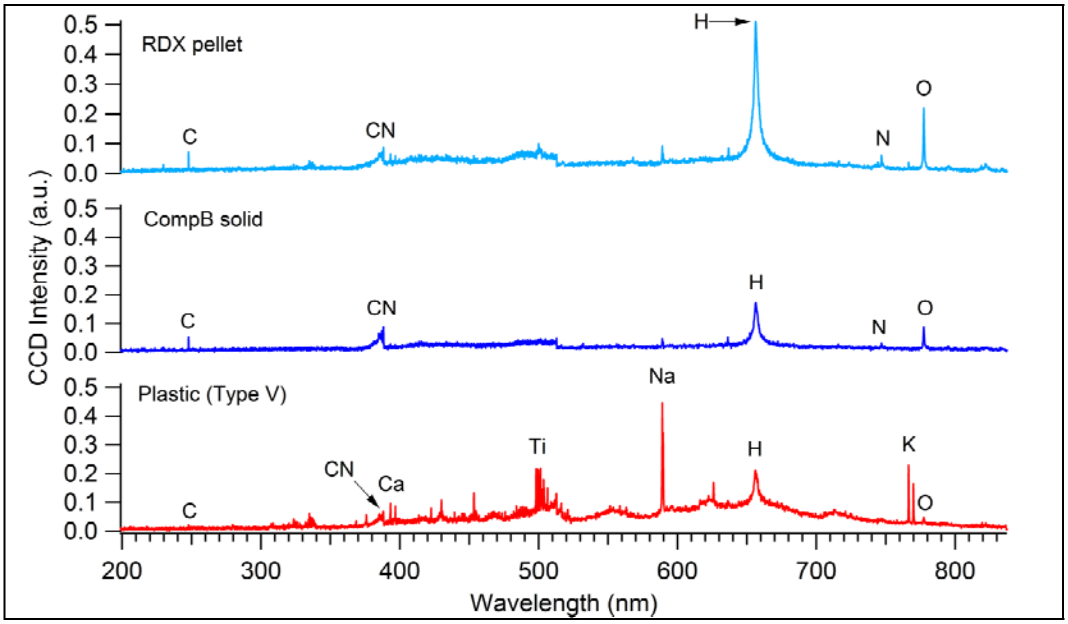

Figure 7. Single-shot spectra of various organic materials acquired at 20 m with the second generation ST-LIBS double pulse system (~275 mJ per pulse). (Spectra include the energetic materials RDX and composition-B, and a type V white plastic. Strong elemental/molecular lines are identified.)

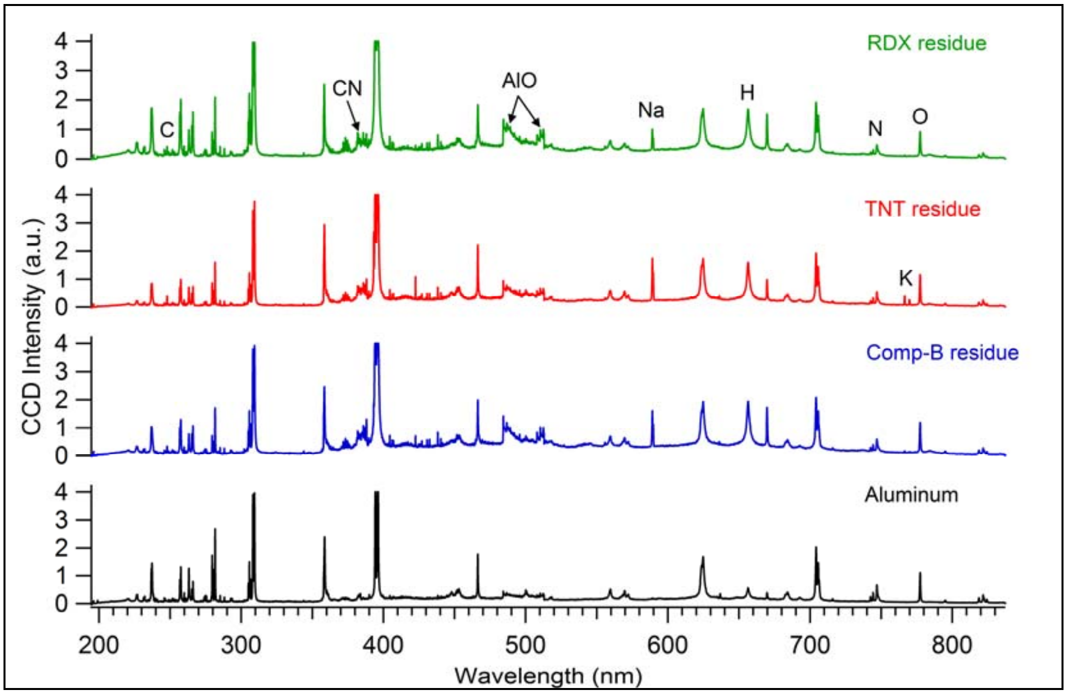

Figure 8. Single-shot spectra (ST-LIBS at 20 m, ~550 mJ total energy) of RDX, TNT and Comp-B residues on an Al substrate (the Al spectrum is shown for comparison). (Strong emission lines of C, CN, AlO, Na, H, N, K, and O are labeled in the spectra. Most unlabeled lines are attributable to Al I and Al II emission.)

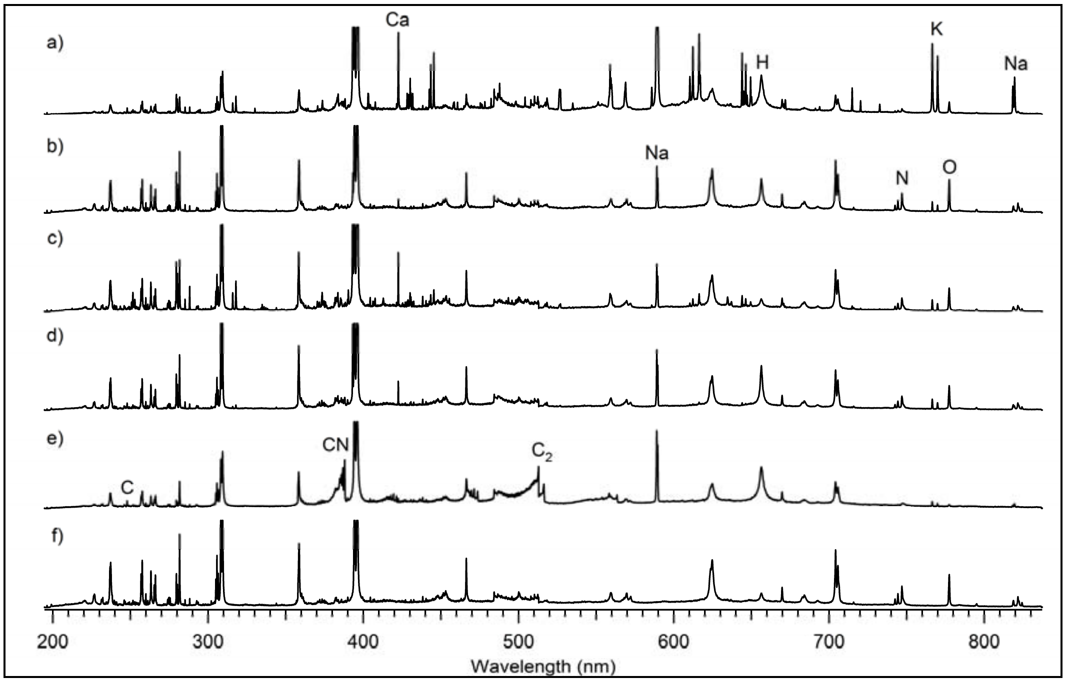

Figure 9. Single-shot spectra (ST-LIBS at 20 m, ~550 mJ total energy) of various biological, inorganic and organic residue interferents on an Al substrate: a) *Bacillus subtilis* (anthrax surrogate), b) *Alternia alternata* (mold), c) Arizona road dust, d) fingerprint residue, e) lubricant oil, and f) Al substrate. (All spectra are shown on the same intensity scale [the Al I lines at 394 and 396 nm are saturating the detector]. Strong emission lines of C, CN, Ca, AlO, C_2, Na, H, N, K, and O are labeled in the spectra. Differences in the spectra are difficult to see by visually [especially with the Al background] but can be efficiently extracted with chemometric techniques.)

successfully identifying explosive-containing mixtures. We have investigated the discrimination ability of our system using techniques such as flow chart analysis, linear correlation, PCA, SIMCA, and PLS-DA.

In an initial field test of an early stand-off LIBS system developed by the Laserna group at the University of Málaga (*2*), a flow chart algorithm was developed to decide whether a sample was an explosive or a non-explosive. All the blind test samples were correctly identified with this data-processing algorithm. A similar algorithm based on 16 conditions describing relative emission intensities was developed and applied to the residue data collected with ARL's ST-LIBS system. In contrast to the Málaga algorithm, none of the criteria depend on specific numbers. If all the following conditions are true (O/C > N/C, O/C > N/CN, H/C > O/H, H/C > C_2/CN, H/C > (O+N)/(C+H), N/C > N/CN, N/C < (O+N)/(C+H), O/H > N/H, C/CN < H/CN, C/CN < C_2/CN, O/CN > N/CN, O/CN > (O+N)/(C+C_2+CN+H), Ca/O < Ca/N, C < CN, C < O, N < O), the sample is classified as an explosive. We calculated the ratios by using summed background-corrected intensities of the C, C_2, CN, H, N, O, Ca, Na, and K lines present in the spectra (table 2). The use of summed intensities rather than single peak intensities results in greater reproducibility among the single-shot spectra. The ratios were chosen so that all 150 of

Table 2. Lines from the explosives spectra used for the discrimination of sample residues (the background-corrected peak intensities of each atomic/molecular species were added to give summed peak intensities for C, C_2, CN, H, N, O, Ca, Na, and K). (The only additional species present in the explosives spectra were attributable to the substrate [Al I-II, AlO].)

Wavelength	Peak	RDX	TNT	Comp-B	Al	dust	oil	fingerprint	AA	BG
247.890	C I	x	x	x	—	—	x	x	x	x
833.715	C I	x	x	x	—	—	x	x	x	x
467.752	C_2	—	—	—	—	—	x	—	—	—
468.370	C_2	—	—	—	—	—	x	—	—	—
469.656	C_2	x	x	x	—	—	x	—	—	—
471.403	C_2	x	x	x	—	—	x	—	—	—
473.608	C_2	x	x	x	—	—	x	—	—	—
512.941	C_2	x	x	x	—	—	x	—	—	—
516.351[a]	C_2	—	—	—	—	—	x	—	—	—
558.416	C_2	—	—	—	—	—	x	—	—	—
563.466	C_2	—	—	—	—	—	x	—	—	—
384.821	CN	x	x	x	—	—	x	—	x	x
385.205	CN	x	x	x	—	—	x	—	x	x
385.863	CN	x	x	x	—	—	x	x	x	x
386.850	CN	x	x	x	—	—	x	x	x	x
388.055	CN	x	x	x	—	—	x	x	x	x
415.002	CN	—	—	—	—	—	x	—	—	—
415.592	CN	—	—	—	—	—	x	—	—	—
416.611	CN	—	—	—	—	—	x	—	—	—
417.898	CN	—	—	—	—	—	x	—	—	—
419.504	CN	—	—	—	—	—	x	—	—	—
421.428	CN	—	—	—	—	—	x	—	—	—
789.522	CN	—	—	—	—	—	x	—	x	x
656.459	H I	x	x	x	x	x	x	x	x	x
742.468	N I	x	x	x	x	x	x	x	x	x
744.366	N I	x	x	x	x	x	x	x	x	x
747.000	N I	x	x	x	x	x	x	x	x	x
777.367	O I	x	x	x	x	x	x	x	x	x
315.881	Ca II	—	—	—	—	x	—	x	x	x
317.946	Ca II	—	—	—	—	x	—	x	x	x
393.192	Ca II	x	x	x	—	x	x	x	x	x
422.550	Ca I	x	x	x	x	x	x	x	x	x
766.516	K I	x	x	x	—	x	x	x	x	x
769.964	K I	x	x	x	—	x	x	x	x	x
589.041	Na I	x	x	x	—	x	x	x	x	x
589.709	Na I	x	x	x	—	x	x	x	x	x
818.282	Na I	—	—	—	—	x	x	x	x	x

[a]The strongest C_2 line occurs at the edge of a spectrometer channel and appears only when the C_2 emission is extremely intense.

the RDX, TNT, and Comp-B residue samples are classified as explosives according to these criteria. In order to confirm the validity of the criteria for explosive samples, ST-LIBS spectra of an additional 26 RDX residue samples were acquired on a separate day, one month later, and were identified as explosives based on the 16 criteria (0% false negatives).

Less than 2% of the interferent samples (Al, Arizona road dust, lubricant oil, fingerprint, mold, BG) resulted in false positives with this algorithm. Four of the five mis-classified spectra belonged to fingerprint residue samples (the other was BG). Unfortunately, the algorithm did not perform well for mixtures containing RDX. Only one of the RDX+dust mixture samples was correctly identified as an explosive (99% false negatives), although none of the oil+dust samples resulted in false positives. Despite the algorithm's success with pure materials, a more sophisticated algorithm is required for real-world applicability.

Linear correlation is a simple measure of the strength of the relationship between two variables. ARL has successfully applied linear correlation to the discrimination of biomaterial powders detected on indoor surfaces with the MP-LIBS (*3*). For the current experiment, a library of 50 spectra each of RDX, TNT, Al, dust, and oil was created and the correlation tool in the Analysis Toolpak of Microsoft Excel was used to test each of the RDX, TNT, Al, dust, and oil spectra individually against the library (the sample spectrum being tested was temporarily removed from the library for the calculation).

The results of the highest correlation match, generated with the entire broadband spectra, are given in table 3. All spectra of the five samples in the library were correctly identified, indicating that the sample spectra were reproducible for this data set. The Comp-B residue spectra were also tested against the library, which correctly identified all the samples as explosives (RDX or TNT). A comparison of the fingerprint residues to the library resulted in a large number of false positives (98%), however. Linear correlation was able to correctly classify 94% of the RDX+dust (acetone) mixtures as explosives, but only 4% of the RDX+dust (crushed) samples were correctly classified.

A second library was constructed with nine summed peak intensities (C, C_2, CN, H, N, O, Ca, Na, and K) and 20 intensity ratios (O/C, H/C, O/N, N/C, O/H, N/H, C/CN, O/CN, H/CN, N/CN, C_2/CN, C_2/C, (O+N)/(H+C), Ca/H, Ca/C, Ca/O, Ca/N, (O+N)/(C+C_2+CN+H), (O/N)/(H/C), and CN/(N/C)) rather than the entire spectra, which contain emission lines from the substrate in addition to those from the sample residue. The results of the linear correlation with this abbreviated data set are given in table 4. The percentage of correct identifications with this method is lower for the RDX, Comp-B, and the RDX+dust mixtures than those obtained with the entire spectra. Since the summed intensities and ratios reflect the composition of the sample residues, this means that the linear correlation with the entire spectra depends on intensity information from the substrate/background to improve the classification of unknown samples. For this reason, linear correlation is unlikely to be effective for identifying residues on different substrates.

Table 3. Results of linear correlation with the entire spectra. (Fifty single-shot spectra of each unknown were tested against a library containing 49 or 50 spectra each of RDX, TNT, Al, dust, and oil. The 50 unknown samples of RDX, TNT, Al, dust, and oil were removed from the library one at a time and tested against the remaining spectra in the library.)

Unknown Sample	Number of Matches With the Strongest Correlation					Correct ID	False Positives	False Negatives
	RDX	TNT	Al	Dust	Oil			
RDX	50	0	0	0	0	100%	—	0%
TNT	0	50	0	0	0	100%	—	0%
Al	0	0	50	0	0	100%	0%	—
Arizona dust	0	0	0	50	0	100%	0%	—
lubricant oil	0	0	0	0	50	100%	0%	—
Composition-B	11	39	0	0	0	100%	—	0%
fingerprint residue	44	5[a]	1[b]	0	0	—	98%	—
RDX+dust mix (acetone)	0	47	0	3	0	94%	—	6%
RDX+dust mix (crushed)	0	2	0	48	0	4%	—	96%
oil+dust mix	0	0	0	50	0	—	0%	—

[a]Three of the samples had Al ranked 2-5.
[b]The sample had dust ranked 2-5.

Table 4. Results of linear correlation with nine summed peak intensities (C, C_2, CN, H, N, O, Ca, Na, and K) and 20 ratios (see text).

Unknown Sample	Number of Matches With the Strongest Correlation					Correct ID	False Positives	False Negatives
	RDX	TNT	Al	Dust	Oil			
RDX	49	0	0	1	0	98%	—	2%
TNT	0	50	0	0	0	100%	—	0%
Al	0	0	50	0	0	100%	0%	—
Arizona dust	0	0	0	50	0	100%	0%	—
lubricant oil	0	0	0	0	50	100%	0%	—
Composition-B	32	17	0	0	1[a]	98%	—	2%
fingerprint residue	38	7	3	2	0	—	90%	—
RDX+dust mix (acetone)	16	6	1	27	0	44%	—	56%
RDX+dust mix (crushed)	0	0	0	50	0	0%	—	100%
oil+dust mix	0	0	0	50	0	—	0%	—

[a]TNT was ranked fifth.

PCA is a chemometric technique for data reduction, which groups variables into principal components that describe trends within the data set. The scores extracted for each principal component (PC) describe the variation of each sample in the model. PCA has previously been applied by our group to LIBS spectra of bioagent simulants and interferents (*4*). For our initial analysis of the stand-off data, the six ratios of the C, H, N, and O peak intensities (H/C, N/C, O/C, N/H, O/H, and O/N) were calculated for each individual spectrum, and the data from five samples (Al, RDX residue, lubricant oil, Arizona road dust, and fingerprint residue; 50 spectra each) were analyzed with PCA. The model was built with three principal components that describe 65% (PC1), 25% (PC2) and 8.9% (PC3) of the total variance within the data set. The

PCA scores for each PC represent weighted sums of the original variables. Figure 10 is a scores plot relating the scores along the first two principal components (PC1 and PC2) for the five samples. Each symbol on the plot represents a single-shot spectrum of the sample. With only a few exceptions, each sample type groups separately from the other sample groups. One fingerprint residue spectrum clusters with the Al substrate, indicating that the laser likely hit an area of the Al without any residue. Everything within the ellipse in figure 10 (arbitrarily drawn to enclose as many RDX samples as possible while excluding interferents) is classified as an explosive with this model, while the samples that fall outside the ellipse are classified as non-explosive. Two spectra of RDX residue cluster with the fingerprint residue outside the ellipse. Although perfect separation of the sample groups (i.e., no overlap between sample clusters) can be achieved if we include ratios of peaks that are characteristic of the interferents in the PCA analysis, our model is designed to be independent of the specific interferents used since it looks only at the elements present in the explosive (C, H, N, O).

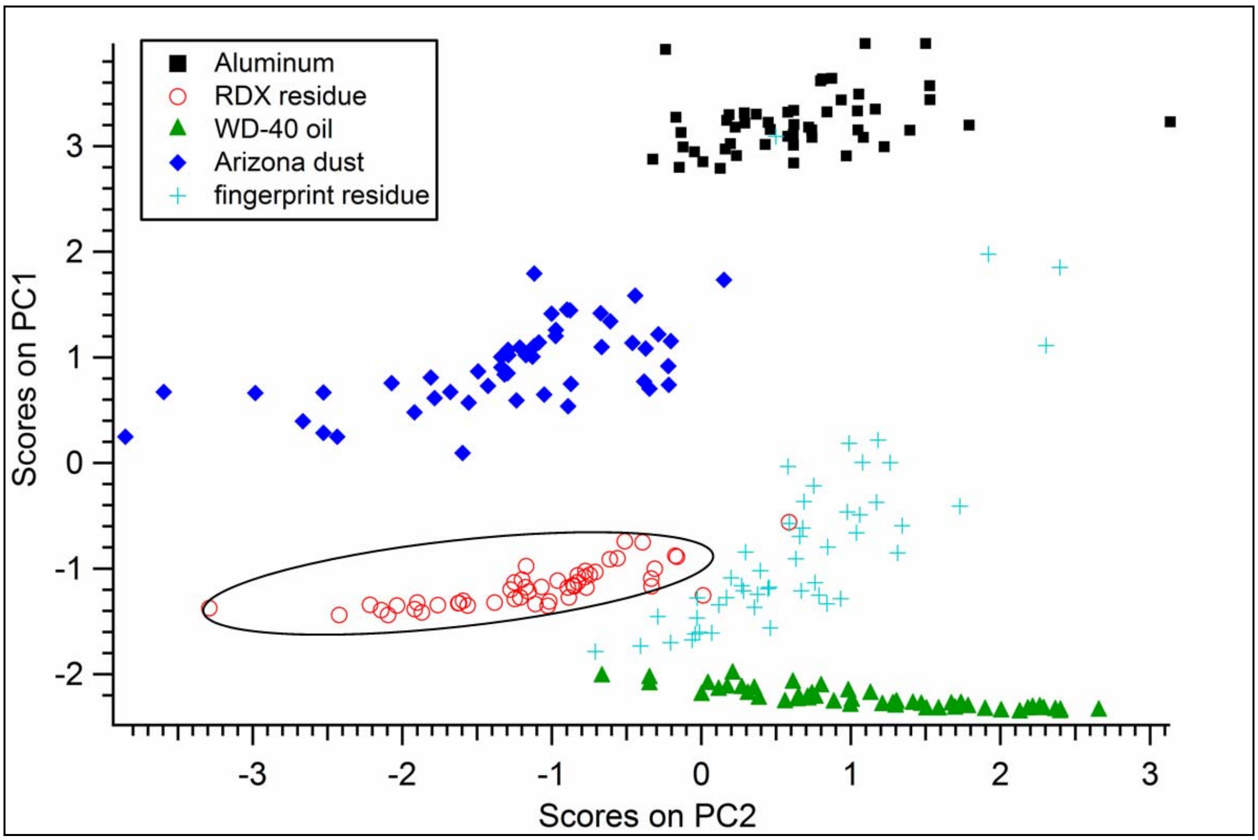

Figure 10. PCA scores plot of Al and RDX, oil, dust, and fingerprints on Al. (Each symbol represents one spectrum described by six ratios of the key elements C, H, N, and O. Fifty spectra of each sample were used to construct this plot. All samples within the ellipse are classified as an explosive, while everything outside the ellipse is classified as non-explosive.)

One way of evaluating the performance of a system is through the use of a receiver operating characteristics (ROC) curve. In a ROC curve, the sensitivity (the fraction of true positives) vs. 1-specificity (where specificity is the fraction of true negatives) is graphed. Figure 11 shows the ROC curve for the discrimination of RDX residues on Al vs. the interferents (Al substrate, fingerprint residue, oil residue, and dust) with peak intensities or ratios of C, H, N, and O. The diagonal line represents a completely random predictor of explosive/no explosive. The ideal detector has 100% sensitivity (no false negatives) and 100% specificity (no false positives). We calculated the sensitivity and specificity at each point by varying the size of the ellipse in figure 10 (a similar PCA scores plot was constructed with the peak intensities of C, H, N, and O instead of the ratios). Using peak intensities gives 78% sensitivity with 0% false positives and 16.5% false positives with 100% sensitivity, while using peak ratios gives 96% sensitivity with 0% false positives and 4% false positives with 100% sensitivity. Therefore, using peak ratios rather than intensities provides better discrimination with PCA for explosives detection with ST-LIBS. One reason for the improvement is that using peak ratios significantly decreases the effect of shot-to-shot variations in laser energy, plasma temperature, material ablation, etc.

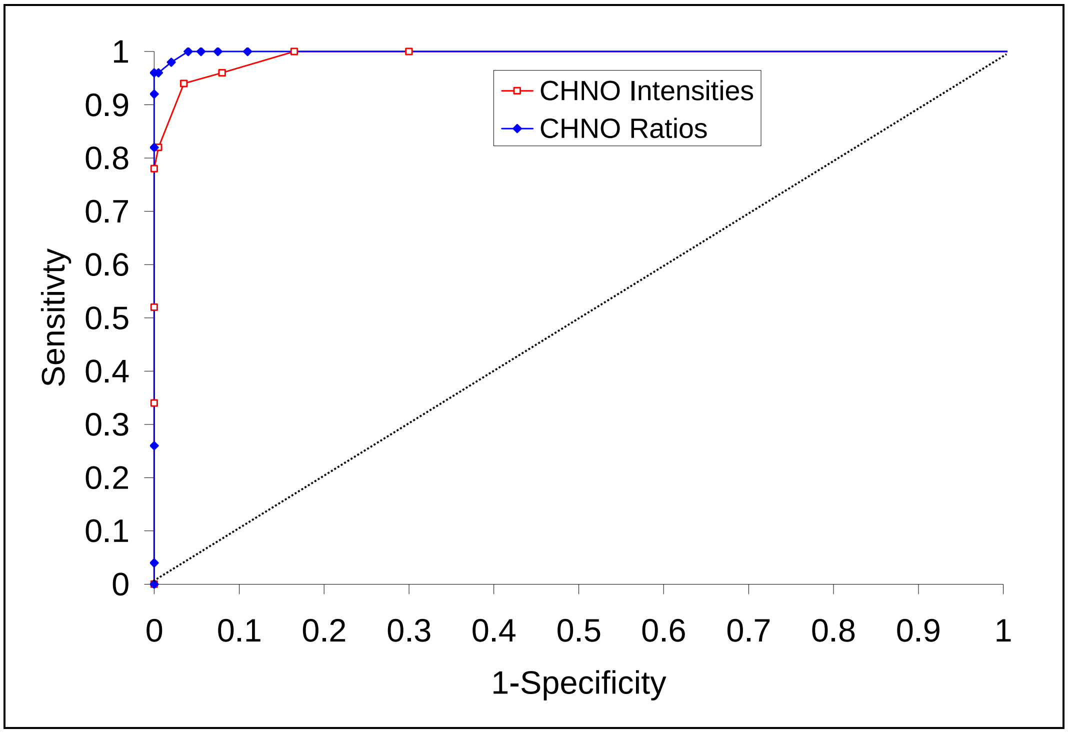

Figure 11. ROC curve for the discrimination of RDX residues on Al vs. the interferents (Al substrate, fingerprint residue, oil residue, and dust) with peak intensities or ratios of C, H, N, and O. (We calculated the sensitivity [true positives] and specificity [true negatives] by varying the size of the ellipse in figure 10. Using peak intensities gives 78% sensitivity with 0% false positives and 16.5% false positives with 100% sensitivity, while using peak ratios gives 96% sensitivity with 0% false positives and 4% false positives with 100% sensitivity.)

A more complete separation of the different samples based on the six ratios can be visualized with a three-dimentional PCA scores plot (figure 12). The three explosive residues (RDX, TNT, and Comp-B) group together with this model but are isolated from the interferent sub-groups. No overlap exists between any of the interferent groups, although several of the fingerprint residues group near the blank Al substrate samples (indicating that the plasma sampled an area without any detectable fingerprint residue). A closer look at the loadings for the principal components shows that the O/N and H/C ratios load most significantly into PC1 and are anti-correlated. PCA thus provides a useful tool for identifying whether samples are the same or different and what variables are responsible for the differences.

Greater sample group separation can be achieved if the broadband nature of the acquired LIBS spectra is employed. Using the nine summed intensities and 20 ratios discussed earlier (p. 13) should provide much better separation between the sample sets. In order to account for greater than 99% of the variance with PCA with the 29 variables (as in the first example with only six variables and three principal components), 13 principal components are required. Consequently, the sample groupings are challenging to visualize in two or three dimensions.

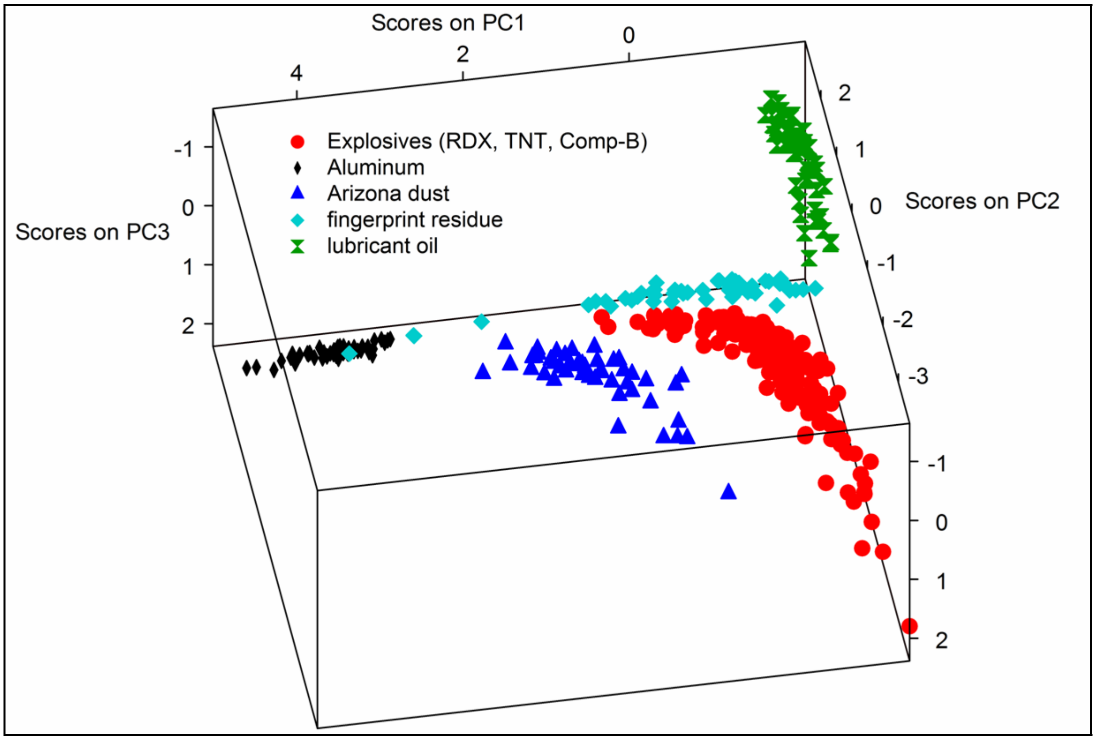

Figure 12. PCA scores plot of explosive residues and interferents (50 samples each) constructed with the ratios O/N, O/C, H/C, N/C, O/H, and N/H. (The strongest emission lines for each element [C 247 nm, H 656 nm, N 747 nm, and O 777 nm] were used for the background-corrected peak intensities. The explosive residues [RDX, TNT, and Comp-B] overlap with each other but form an isolated group separate from the interferent groups. No overlap exists between any of the groups with the first three principal components, except for several of the fingerprint residues that group near the blank Al substrate samples [indicating that the plasma sampled an area without any detectable fingerprint residue].)

An alternate approach is to use the SIMCA, which consists of a collection of PCA models, one for each modeled class in the data set. Each PCA model has an independently determined number of PCs that describe the variance within the class. The SIMCA model can then be used to determine the identity of unknown samples. A SIMCA model was built with 50 spectra each (represented by nine summed peak intensities and 20 ratios) of RDX and TNT (class 1, 8 PC), Al (class 2, 5 PC), Arizona dust (class 3, 7 PC), and lubricant oil (class 4, 8 PC). "Unknown" samples (50 each) of Comp-B, fingerprint residue, RDX+dust (acetone), RDX+dust (crushed), and an oil+dust mixture were tested against the model. The results of these tests are shown in figure 13. Although the model correctly classified all the Comp-B samples and many of the RDX+dust samples as explosives, most of the fingerprint residue samples and several of the oil+dust samples were incorrectly classified as explosives (false positives). The main disadvantage of SIMCA is that the PCA models are computed with the goal of capturing intra-class variations without consideration of inter-class differences.

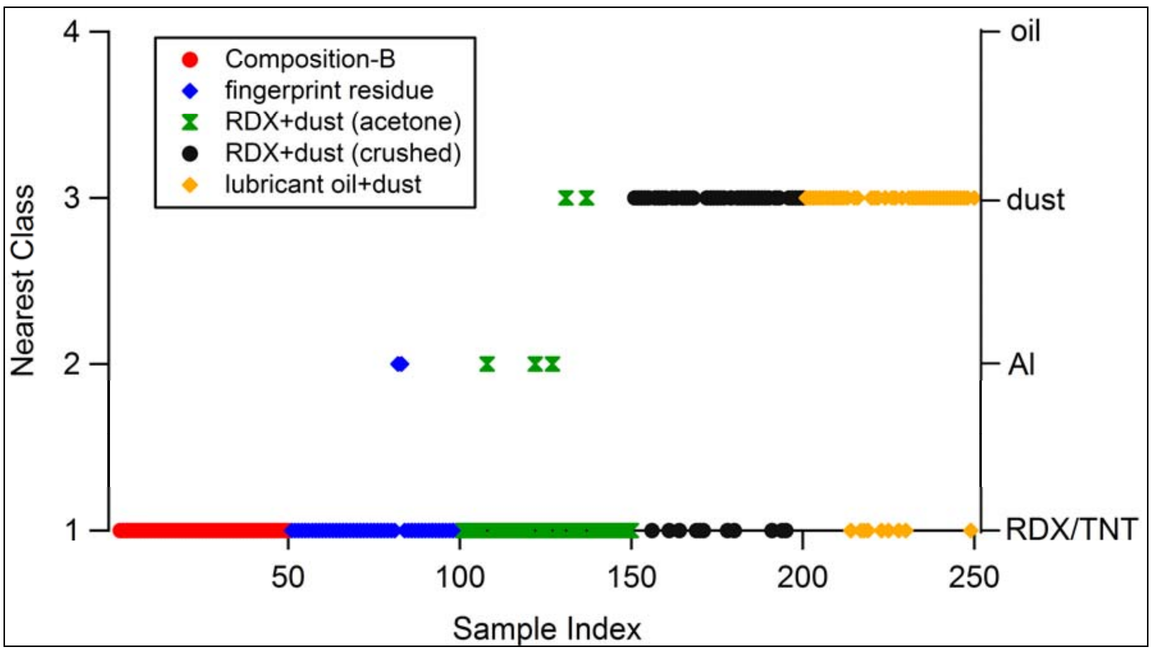

Figure 13. Results of "unknown" samples (50 each) of Comp-B, fingerprint residue, RDX+dust mixed in acetone and deposited on the Al substrate, RDX+dust crushed directly on the Al, and oil+dust smeared on Al tested against a SIMCA model built with 50 spectra each (represented by nine summed peak intensities and 20 ratios) of RDX and TNT (class 1), Al (class 2), Arizona dust (class 3), and lubricant oil (class 4). (The SIMCA model predicted the nearest class of the unknown sample, based on the known samples in the model. Most of the fingerprint residue samples and several of the oil+dust samples were incorrectly classified as explosives [false positives], while a significant number of the RDX+dust samples were classified as dust rather than RDX [probable false negatives].)

PLS-DA is a multivariate inverse least squares discrimination method used to classify samples. Unlike SIMCA, partial least squares generates predictor variables (called latent variables or LVs) while attempting to capture variance and achieve correlation. The model predicts the class

number for each sample, based on a value of 0 to 1. A value closer to 0 indicates that the sample is not in the modeled class, while a value of 1 indicates that the sample is a member of the modeled class. A threshold between 0 and 1 (above which a sample is considered in the class) is automatically calculated by the software with Bayesian statistics in order to minimize the number of false positives and false negatives. The number of LV chosen to be included in each of the models described next was confirmed with cross validation ("leave one out" method) to minimize the root mean square (rms) error.

The choice of variables to represent each spectrum was critical for enhancing the classification ability of the PLS-DA model. Using the entire broadband spectrum for constructing the model worked extremely well for the sample types included in the model, but unknown samples that did not belong to the original model were predicted to belong to each of the classes in the model with roughly equal probability. Different combinations of intensities and/or ratios based on peak intensities (or areas) of single lines or summed intensities of species found in the explosives spectra C, H, N, O, C_2, CN, and the impurities Ca, Na, and K were tested. The combination of nine summed intensities and 20 ratios previously described was found to provide the best discrimination for all the PLS-DA models, based on our data set. Models built with only the nine summed intensities or just the 20 ratios performed nearly as well (with a few false positives and false negatives that are eliminated when both intensities and ratios are used).

Figure 14 demonstrates discrimination of the RDX, TNT, and Comp-B residues (50 spectra each) with PLS-DA. A PLS-DA model based on nine summed peak intensities and 20 ratios was developed (18 LV). Excellent discrimination of the explosive samples was achieved (with the Bayesian thresholds shown in the figure), although some overlap between the RDX and Comp-B occurs because of the high percentage of RDX in Comp-B. These results show that discrimination among different types of explosives is possible with LIBS, despite their similar elemental compositions (*1*).

When all the explosive, Al, dust, oil, and fingerprint residue spectra were used to create a PLS-DA model with 17 LV based on the nine summed peak intensities and 20 ratios, almost perfect classification of the samples was achieved (figure 15). Two fingerprint residue samples were predicted to belong to the same class as Al; a visual inspection of those spectra confirms that no carbon and very little hydrogen are present, indicating that the plasma most likely sampled an area that contained no fingerprint residue. Because application of the fingerprint residue to the Al results in channels of residue corresponding to the ridges of a human fingerprint (*5*), this result is not too surprising. In addition, one of the Al samples was predicted to be a fingerprint residue. It is quite possible that the plasma sampled an area of the Al accidentally contaminated with fingerprints. Most importantly, the model predicts no false positives and no false negatives for explosive samples.

Despite the encouraging success of PLS-DA for classifying explosive residues, for real-world applications, it would be impossible to include every possible environmental interferent in the

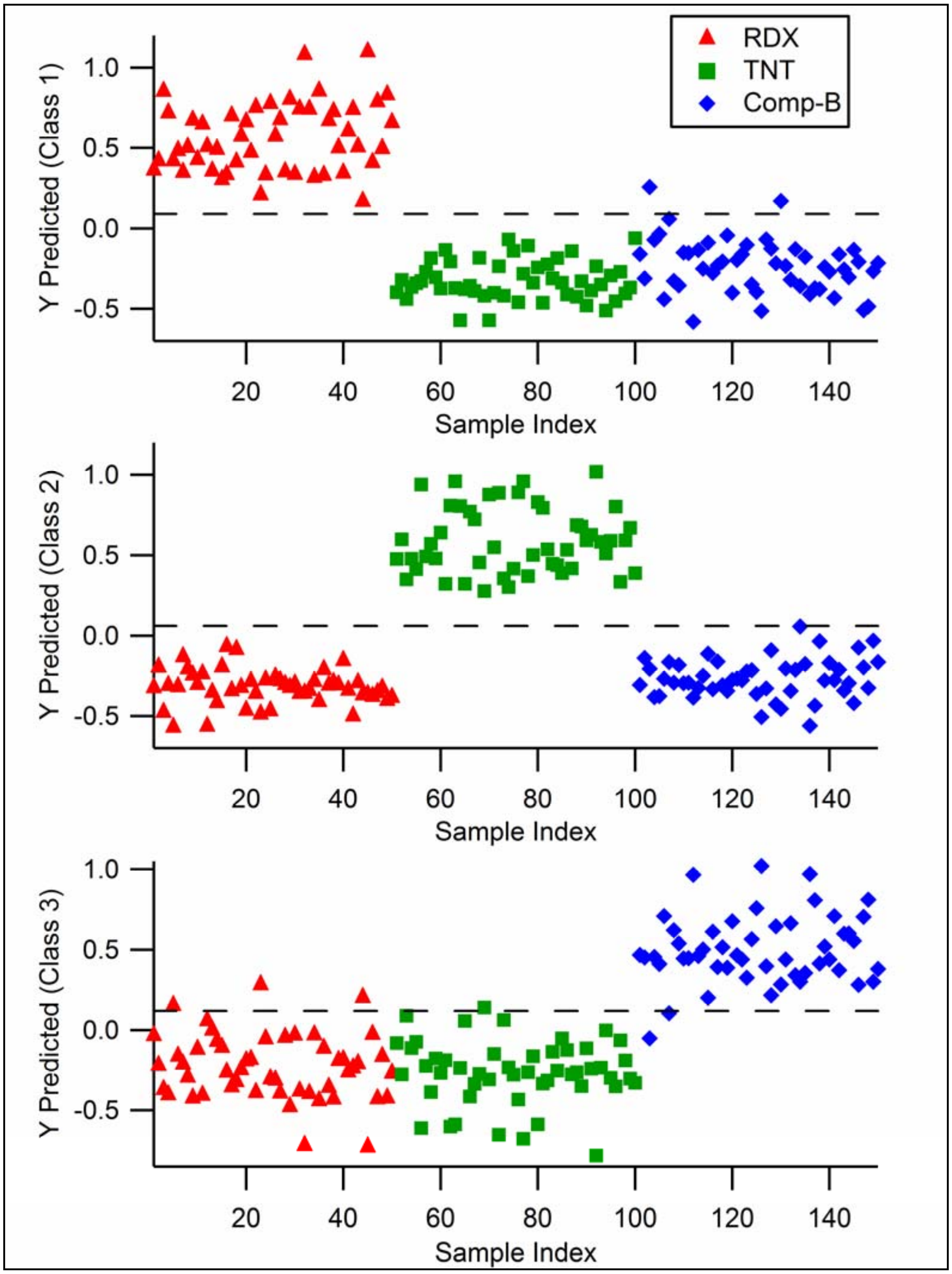

Figure 14. Discrimination of different explosive residues with PLS-DA. (Fifty spectra of RDX, TNT, and Comp-B [63% RDX, 36% TNT, 1% wax] on Al were acquired and a PLS-DA model based on nine summed peak intensities and 20 ratios was developed. Excellent discrimination of the samples was achieved, although some overlap between the RDX and Comp-B occurs because of the high percentage of RDX in Comp-B.)

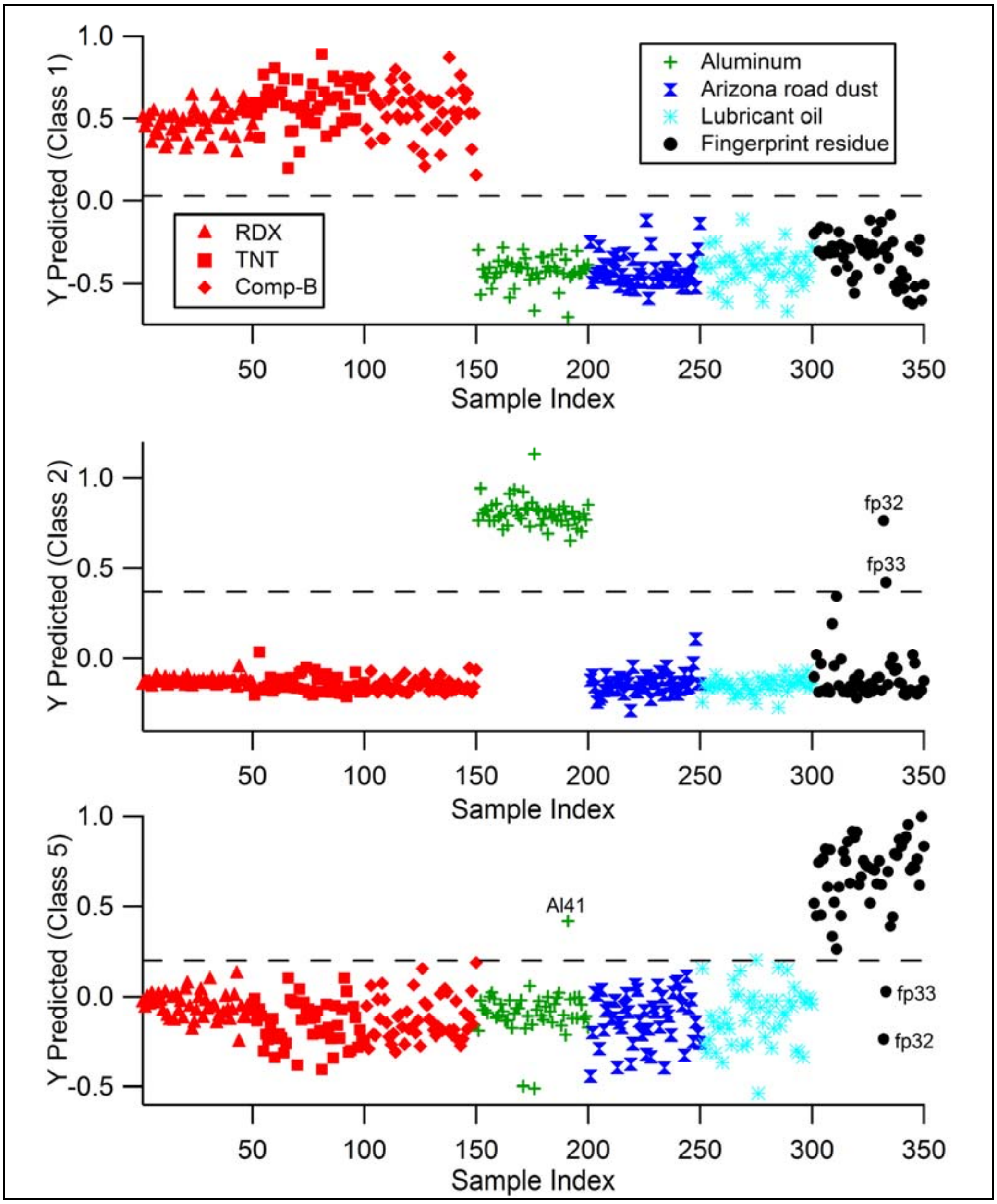

Figure 15. PLS-DA model showing the classification of samples with nine summed intensities and 20 ratios. (All explosive [samples 1-150, class 1], Arizona road dust [151-200, class 3], and oil [201-300, class 4] samples class correctly [i.e., the predicted score is above the Bayesian threshold calculated by the model for each class]. Fingerprint residues #32 and #33 group with Al as class 2 [visual inspection of the spectra confirm that the plasma did not sample a detectable amount of residue]; Al #41 most likely contained some fingerprint residue [class 5].)

model. In order to test the ability of PLS-DA to deal with samples (explosive and non-explosive) not included in the original model, a model was developed based on RDX, TNT, Al, dust, and oil (20 LV, nine summed intensities and 20 ratios). The spectra of Comp-B and fingerprint residue were then tested against the model, which predicted the classification of the

“unknown” test samples (figure 16). With the Bayesian threshold calculated by the model, a significant number of the fingerprint residues registered as false positives. Because the position of the threshold can be arbitrarily selected, based on the number of false positives and false negatives the user is willing to accept, the threshold can be chosen as shown in figure 16 so that all but one of the Comp-B samples and none of the fingerprint residues register as explosives. The remainder of the fingerprint residue samples are classified by the model as oil (11 samples), Al (4 samples), or dust (3 samples) according to the Bayesian thresholds.

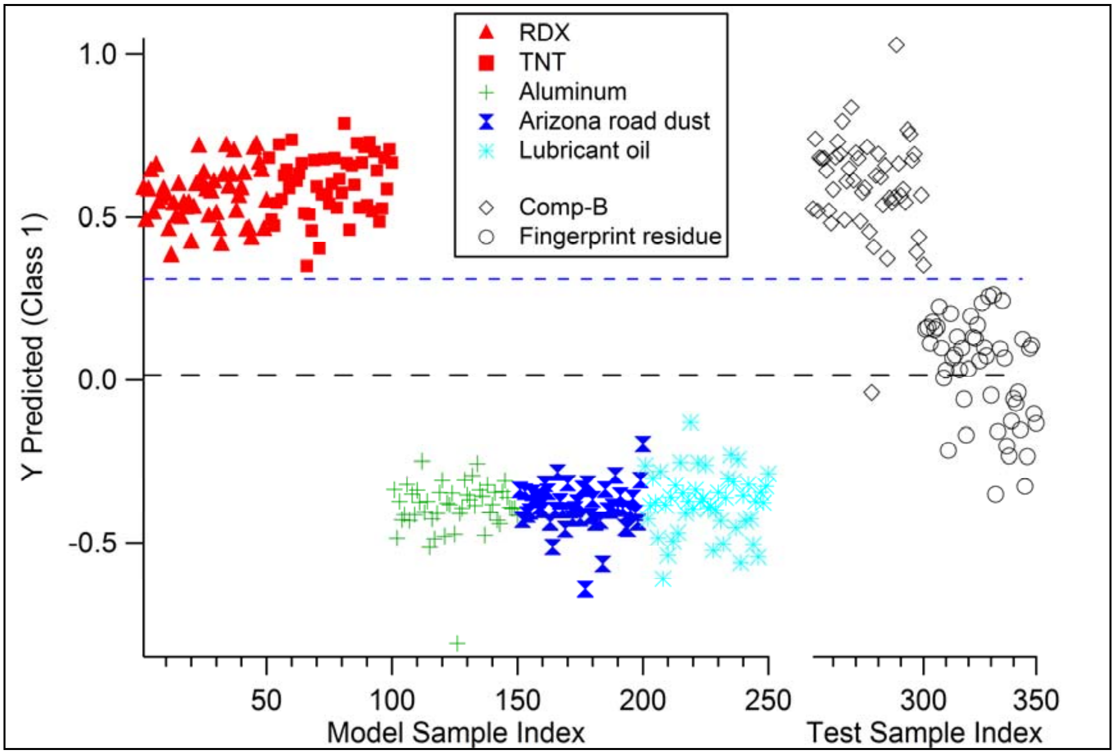

Figure 16. PLS-DA model built on RDX (samples 1-50), TNT (51-100), Al (101-150), Arizona road dust (151-200), and oil (201-250). (“Unknown” samples of Comp-B [251-300] and fingerprint residue [301-350] were tested against the model to determine how well the model handles substances not in the model. With a user-specified threshold [blue dashed line], Comp-B was correctly identified as an explosive [except for one sample] and all the fingerprints were identified as non-explosives [classified as oil, Al, or dust].)

Another important issue in real-world applications is the ability of the model to recognize explosives in the presence of interferents. A PLS-DA model based on RDX, Al, and dust was created with the nine summed intensities and 20 ratios (6 LV). The RDX+dust mixtures (dissolved in acetone or crushed directly on the Al) and the oil+dust mixture spectra were tested against the model. All the RDX+dust (acetone) samples and more than half of the RDX+dust (crushed) samples were classified as RDX (table 5). Because the RDX+dust (crushed) samples were extremely inhomogeneous, it is likely that the RDX+dust samples identified by the model as non-explosives represented instances when the laser sampled only dust (i.e., no RDX was

Table 5. Classification results of mixtures of RDX+dust (dissolved in acetone or crushed directly on the substrate, 50 samples each) and oil+dust (50 samples) tested against a PLS-DA model built on RDX, Al, and Arizona dust.

Model Class	**Unknown Samples**		
	RDX+Dust (acetone)	**RDX+Dust (crushed)**	**Oil+Dust**
RDX	100%	66%	0%
Al	0%	0%	0%
Arizona dust	24%	100%	100%

present in the sampling region). Many of the RDX+dust samples were also classified with the pure dust samples, thus demonstrating that the model picked up both components of the mixture. The oil+dust mixture grouped only with the pure dust and did not result in any false positives. These results demonstrate the applicability of this explosive/non-explosive classification method to mixtures.

Finally, a PLS-DA model was constructed with RDX, TNT, Al, dust, oil, mold (AA), and BG (20 LV), based on summed intensities for C, N, O, H, C_2, CN, Ca, Na, K, Ba, Li, Mg, Mn, Sc, Si, and Sr, and 23 intensity ratios (O/C, H/C, O/N, N/C, O/H, N/H, C/CN, O/CN, H/CN, N/CN, C_2/CN, C_2/C, (O+N)/(H+C), Ca/H, Ca/C, Ca/O, Ca/N, (O+N)/(C+C_2+CN+H), (O/N)/(H/C), CN/(N/C), Mg/Mn, Si/Li, (Sr+Sc)/Ba). These intensities and ratios were chosen, based on the peaks present in the LIBS spectra of the hazards of interest (explosives and the anthrax surrogate BG). Table 6 lists the lines observed in the bio-residue spectra, including those used for the summed intensities.

The correct explosive/non-explosive classification of the Comp-B and fingerprint samples (with a user-defined threshold as before) together with the correct classification of the “unknown” anthrax surrogate samples (five additional BG samples not included in the model) demonstrates that simultaneous biohazard and explosive residue discrimination is possible with stand-off LIBS (table 7). Although 88% of the fingerprint residue samples classified as mold, the important result is that they did not classify as explosives despite the fact that the fingerprint residue was not included in the original model. If the user were interested in identifying mold, peak intensities and ratios based on mold would be used to construct the model.

More than 5 months after the initial ST-LIBS data described were acquired, an additional 100 spectra of RDX (crushed), Arizona road dust, and oil were obtained at 20 m. The new data were combined with the earlier data (50 spectra each of RDX, dust, oil, and Al) in a new PLS-DA model (20 LV) in order to determine if our previous results could be reproduced with data collected on different days with another sample set. As before, the background-corrected summed intensities of the C, C_2, CN, H, N, O, Ca, Na, and K lines were used to calculate the 20 ratios. This time, however, the summed intensities were normalized to the total summed intensity in order to minimize differences in the light collection from day to day (because of

Table 6. Lines from the biomaterials spectra *Alternia alternata* (AA) and *Bacillus subtilis* (BG) on Al (excluding lines present in the spectra of the Al substrate).

[nm]	Peak	AA	BG	[nm]	Peak	AA	BG	[nm]	Peak	AA	BG
363.036	?	—	x	558.977	Ca I	x	x	260.584[a]	Mn II	—	x
364.372	?	—	x	559.539	Ca I	x	x	293.324[a]	Mn II	—	x
383.778	?	x	x	585.926	Ca I	x	x	293.930[a]	Mn II	—	x
455.383[a]	Ba II	x	x	610.431	Ca I	x	x	294.922[a]	Mn II	—	x
493.421[a]	Ba II	x	x	612.308	Ca I	x	x	353.144[a]	Mn I	—	x
553.694	Ba I	—	x	616.389	Ca I	x	x	354.734[a]	Mn I	—	x
247.890[a]	C I	x	x	617.050	Ca I	x	x	356.903[a]	Mn I	—	x
833.715[a]	C I	x	x	644.036	Ca I	x	x	401.784[a]	Mn I	—	x
315.881[a]	Ca II	x	x	645.128	Ca I	x	x	405.52[a]	Mn I	—	x
317.946[a]	Ca II	x	x	646.328	Ca I	x	x	408.274[a]	Mn I	—	x
370.648	Ca II	x	x	647.310	Ca I	x	x	475.400[a]	Mn I	—	x
373.693	Ca II	x	x	649.491	Ca I	x	x	476.218[a]	Mn I	—	x
393.192[a]	Ca II	x	x	650.036	Ca I	x	x	476.576[a]	Mn I	—	x
396.951	Ca II	x	x	671.859	Ca I	x	x	478.312[a]	Mn I	—	x
422.657[a]	Ca I	x	x	714.906	Ca I	x	x	482.337[a]	Mn I	—	x
428.249	Ca I	x	x	720.334	Ca I	x	x	330.220	Na I	x	x
428.887	Ca I	x	x	732.747	Ca I	x	x	498.195	Na I	x	x
430.214	Ca I	x	x	388.219[a]	CN	x	x	568.956	Na I	x	x
430.745	Ca I	x	x	418.005[a]	CN	x	x	589.041[a]	Na I	x	x
431.805	Ca I	x	x	419.611[a]	CN	x	x	589.597[a]	Na I	x	x
435.563	Ca I	x	x	438.308	Fe I	x	x	818.385[a]	Na I	x	x
442.520	Ca I	x	x	656.459[a]	H I	x	x	819.512	Na I	x	x
443.465	Ca I	x	x	766.516[a]	K I	x	x	409.569[a]	Sc I	—	x
445.460	Ca I	x	x	769.964[a]	K I	x	x	409.838[a]	Sc I	—	x
457.877	Ca I	—	x	670.885[a]	Li I	x	x	634.520[a]	Sc I	—	x
458.137	Ca I	—	x	277.979[a]	Mg I	x	x	636.273[a]	Sc I	—	x
487.816	Ca I	—	x	279.537[a]	Mg II	x	x	251.623[a]	Si I	—	x
504.197	Ca I	—	x	280.259[a]	Mg II	x	x	288.188[a]	Si I	—	x
518.854	Ca I	—	x	285.198[a]	Mg I	x	x	403.085[a]	Sr I	—	x
526.579	Ca I	x	x	517.262[a]	Mg I	x	x	407.735[a]	Sr II	—	x
527.033	Ca I	—	x	518.399[a]	Mg I	x	x	458.604[a]	Sr II	—	x
534.965	Ca I	—	x	631.890	Mg ?		x	460.729[a]	Sr I	—	x
551.331	Ca I	—	x	259.403[a]	Mn II		x	640.868[a]	Sr I	—	x

[a]Lines used to give summed peak intensities for C, N, O, H, C_2, CN, Ca, Na, K, Ba, Li, Mg, Mn, Sc, Si, and Sr.

Table 7. Classification results of "unknowns" composition-B (50 samples), fingerprint residue (50 samples), and *Bacillus subtilis* (BG, 5 samples) tested against a PLS-DA model built on RDX, Al, Arizona dust, oil, mold (*Alternia alternata*, AA), and BG.

Model Class	Unknown Samples		
	Composition-B	Fingerprint Residue	BG
RDX	100%	0%	0%
Al	0%	8%	0%
Arizona dust	0%	0%	0%
Oil	0%	2%	0%
Mold (AA)	0%	88%	0%
BG	0%	0%	100%

minor changes in the instrument alignment) and to increase the overall reproducibility of the data. The original TNT and Comp-B residue samples were tested against the new model and 100% of the Comp-B samples, and all but one of the TNT samples were classified as explosives based on the RDX in the model (figure 17). Although Comp-B is 63% RDX, the TNT has a different molecular formula than RDX. Despite this, our model was able to correctly identify TNT as an explosive material. The fingerprint residue samples were correctly classified with the oil rather than with the explosives. By including data from multiple days, the discrimination actually improved so that a user-defined threshold was no longer necessary to separate the fingerprints and explosives (as in figure 16).

Additional samples tested against the new PLS-DA model include the interferent house dust (not included in the model) and RDX samples prepared in an acetone mixture, RDX applied directly to the Al with multiple overlapping fingerprints, and individual RDX fingerprints. The RDX samples were all correctly identified as explosives, while the house dust samples were identified as their closest match in the model, Arizona road dust (figure 18). Together with the results in figure 17, these results confirm that our model is sophisticated enough to correctly identify explosive and non-explosive materials that are not included in the model. In addition, we have shown that data from different days (and therefore slightly different experimental conditions and sample preparations) can be combined.

3.4 ST-LIBS Beyond 20 m

On January 25, 2007, the Gen 2 ST-LIBS system was moved to a 100-m indoor test range at the Aberdeen Test Center (ATC). For the first time, we were able to test the system beyond 20 m (the size of our indoor laboratory). Although the Gen 2 system was originally designed to work at stand-off distances as far as 30 m, we were able to acquire LIBS spectra at much longer distances. RDX residue, lubricant oil, fingerprints, Arizona road dust, an oil+dust mixture, and a RDX+dust mixture were prepared on Al, and spectra of the samples (as well as the plain Al substrate) were acquired at 30 m and 50 m. The present section describes this preliminary work at stand-off distances beyond 20 m.

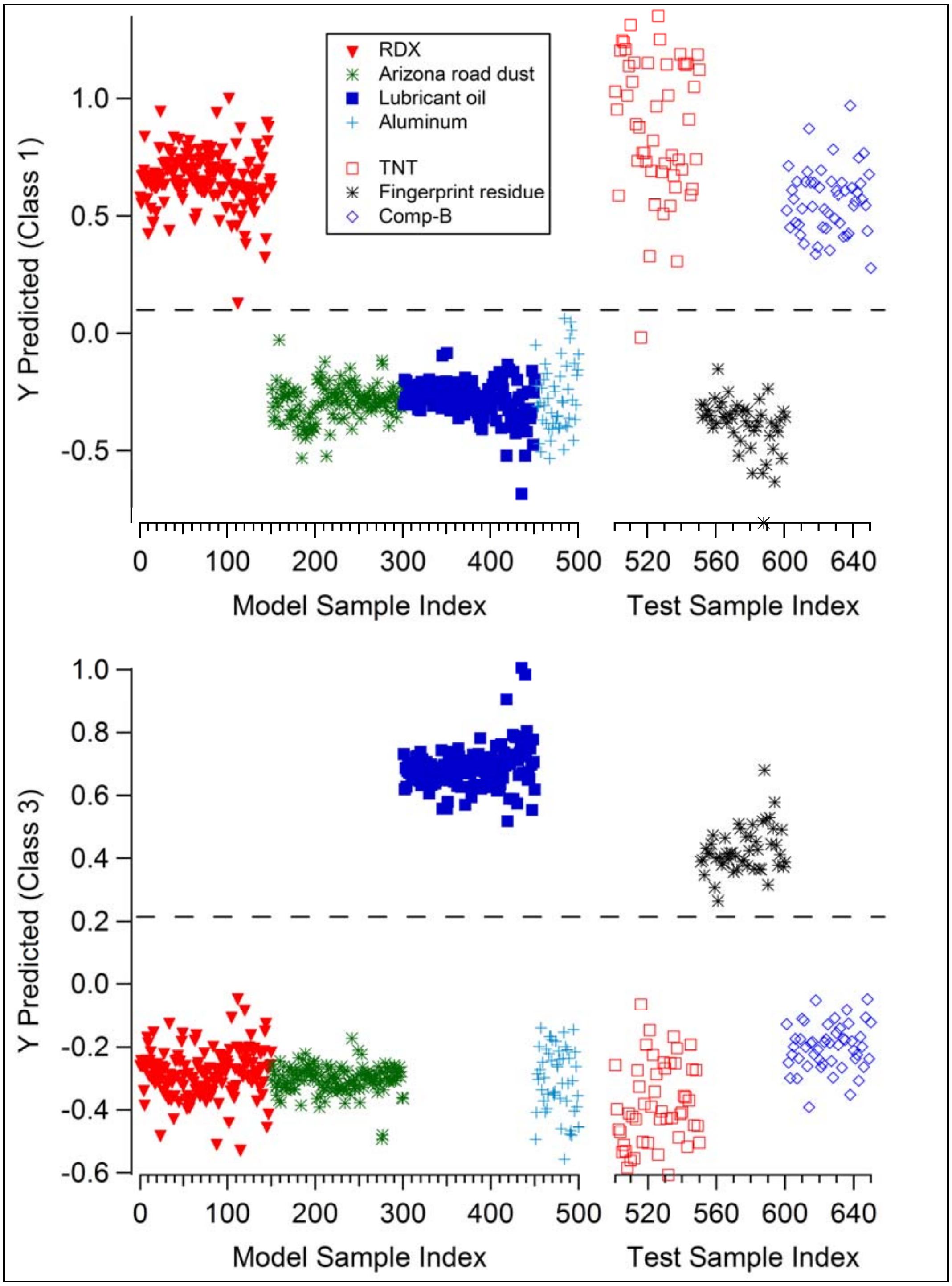

Figure 17. PLS-DA model built with nine normalized summed intensities and 20 ratios for RDX residue (samples 1 through 150), Arizona road dust (151 through 300), lubricant oil (301 through 450) and Al (451 through 500) acquired at 20 m with the ST-LIBS system on several different days. (TNT [501-550], fingerprint [551-600], and Comp-B [601-650] residues were tested against the model, which correctly identified the TNT and Comp-B as explosives [with only one false negative, top] and the fingerprints as oil [bottom], despite the fact that none of the test samples were included in the model.)

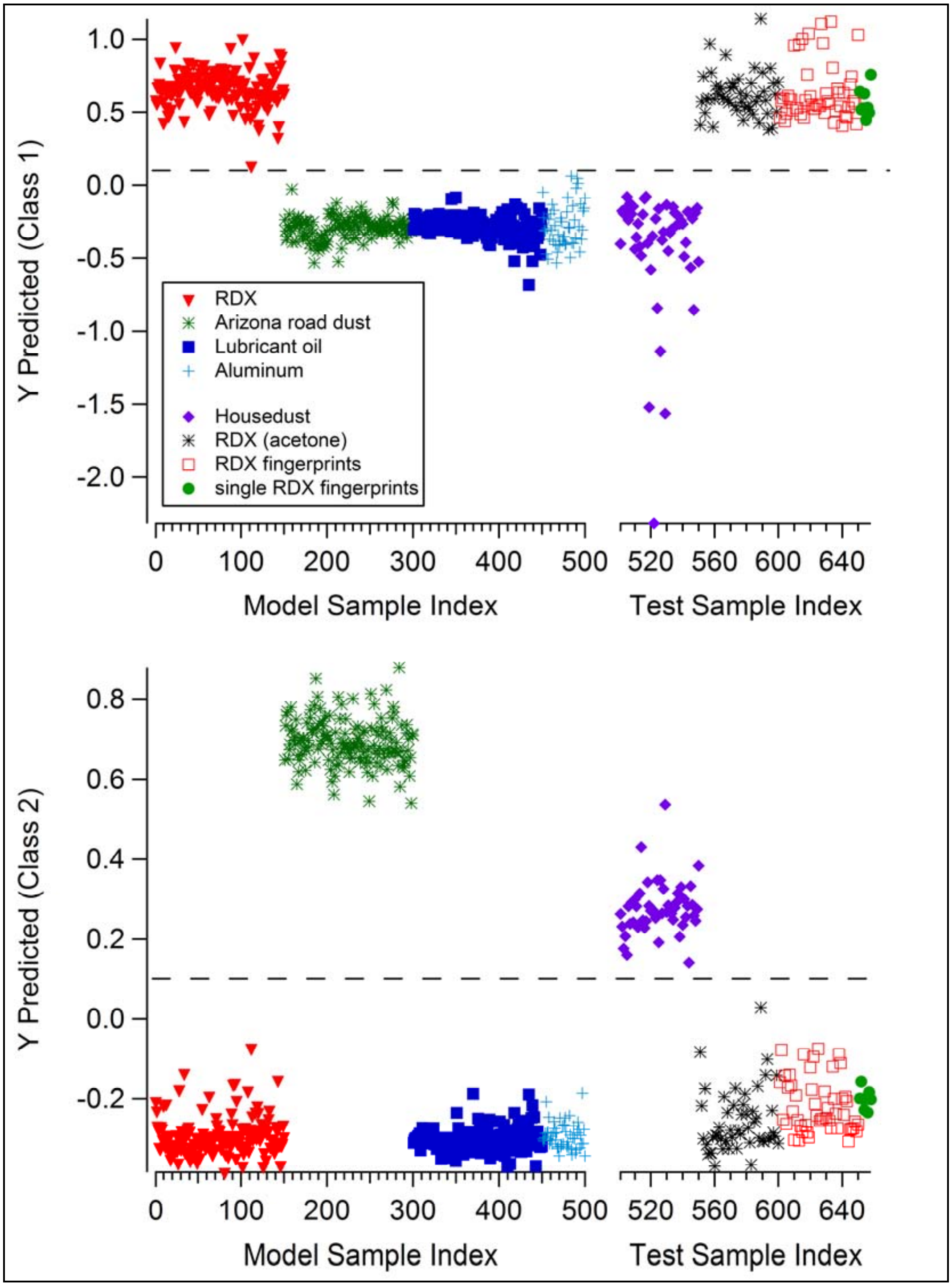

Figure 18. PLS-DA model built with RDX residue (samples 1 through 150), Arizona road dust (151 through 300), lubricant oil (301 through 450) and Al (451 through 500) acquired at 20 m with the ST-LIBS system on several different days. (House dust [501-550], RDX dissolved in acetone [551-600], RDX fingerprints [601-650], and spectra from single RDX fingerprints [651-658] were tested against the model. All the RDX samples were correctly identified as explosives [top], while the house dust was classified with its closest match in the model, Arizona road dust [bottom].)

The ST-LIBS spectra of the residue samples at 30 m are approximately 85% of the intensity of those samples acquired at 20 m (see figures 8 and 9). As shown in figure 19, however, the spectral features that enabled the discrimination of the samples at 20 m are still present (the C line at 247 nm is too weak to see at this scale). A PLS-DA model with 20 LV was built with spectra of Al (50 laser shots), RDX residue (100), lubricant oil (50), Arizona road dust (50) and fingerprint residue (50) acquired at 30 m (figure 20). RDX+dust (50) and oil+dust (50) samples were tested against the model. Only one of the oil+dust samples registered as an explosive (2% false positives), and eight of the RDX+dust samples were not identified as explosives. Because of the inhomogeneous nature of the sample mixtures, it is possible that some or all of the RDX+dust samples contained only dust and were not actually false negatives.

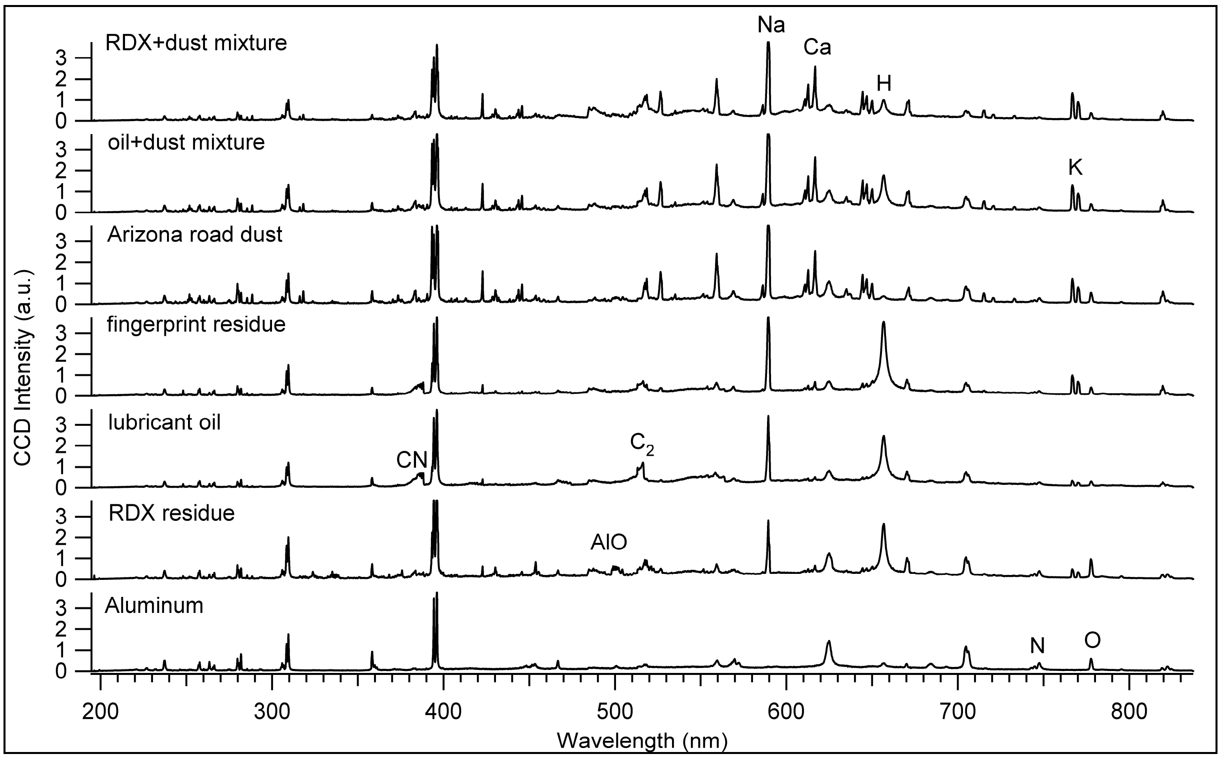

Figure 19. Single-shot spectra of RDX and interferent residues and mixtures on Al acquired at 30 m. (Strong emission lines are labeled [the C line at 247 nm is present but too weak to see on this scale].)

Spectra of the RDX residue and interferent samples were also acquired at 50 m with approximately 25% of the 20-m intensity (figure 21). Despite the dramatic decrease in light collection at 50 m (resulting in no detectable C emission for any of the samples), the single-shot spectra still contain enough spectral detail for us to differentiate between the residues. Figure 22 shows the results of a PLS-DA model (20 LV) built with spectra of Al (20 laser shots), RDX residue (20), lubricant oil (20), and Arizona road dust (25) acquired at 50 m. Fingerprint residue (20), an oil+dust mixture (20) and RDX+dust mixture (20) were tested against the model. None of the fingerprint residues and only two of the oil+dust mixture samples (off-scale) result in false positives (5%). Five of

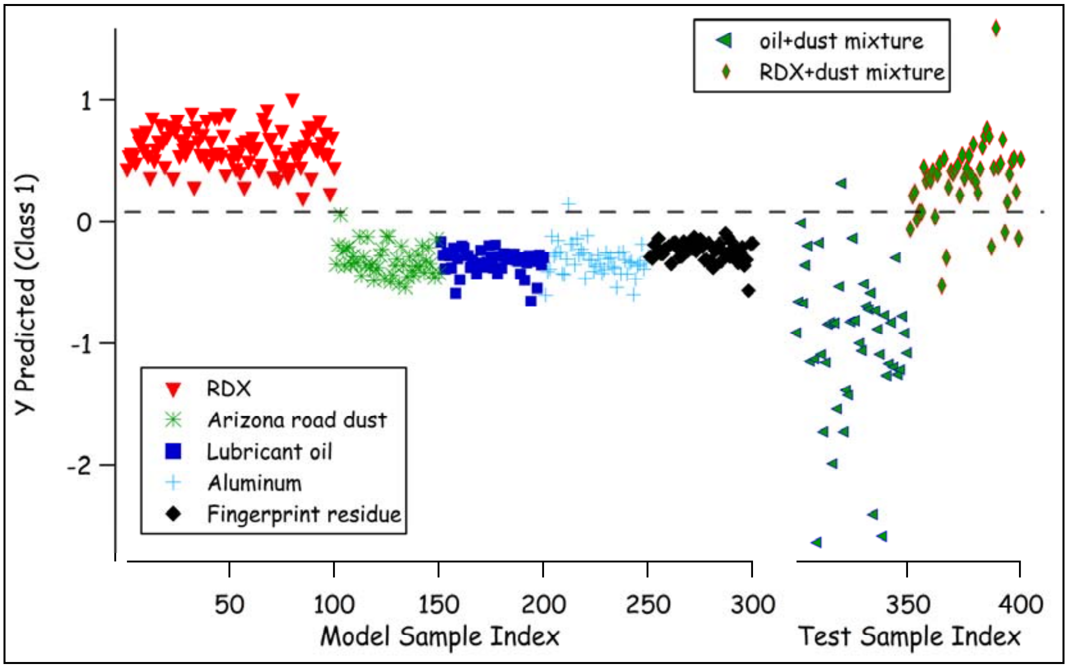

Figure 20. PLS-DA model built with spectra of RDX residue (samples 1 through 100), Arizona road dust (101 through 150), lubricant oil (151 through 200), Al (201 through 250), and fingerprint residue (251 through 300) acquired at 30 m. (An oil+dust mixture [301-350] and RDX+dust mixture [351-400] were tested against the model. Most of the RDX+dust mixture samples were classified as explosives, although about 16% classified only with dust [possible false negatives]. Only 2% of the oil+dust mixture samples resulted in false positives.)

the RDX+dust mixture samples do not classify as explosives and possibly contained only dust in the laser-sampled region. Increasing the number of samples in the library would improve the model and decrease the false negative and false positive rates. However, these initial results demonstrate that detection and discrimination of explosive residues with LIBS is possible at 50 m. Increasing the light collection capability (i.e., using a larger telescope), laser power, and spectrometer sensitivity and modifying the optical design of the stand-off system (optimized for distances beyond 30 m) will improve the maximum stand-off distance for explosives detection.

In order to determine if LIBS spectra acquired at different stand-off distances could be combined in one model, a PLS-DA model was built with 20 LV with spectra (50 samples at 30 m, 20 samples at 50 m) of Al, RDX residue, lubricant oil, fingerprint residue, and Arizona road dust (50 samples at 30 m, 25 samples at 50 m). RDX (50 samples at 30 m), an oil+dust mixture (50 samples at 30 m, 20 samples at 50 m) and RDX+dust mixture (50 samples at 30 m, 20 samples at 50 m) were tested against the model in figure 23. All the additional RDX residue samples were classified as explosives, as were all but nine of the RDX+dust samples (possible false negatives). Six of the oil+dust samples resulted in false positives (8.5%). The use of normalized intensities and intensity ratios appears to reduce any effects in the LIBS spectra caused by the changing of

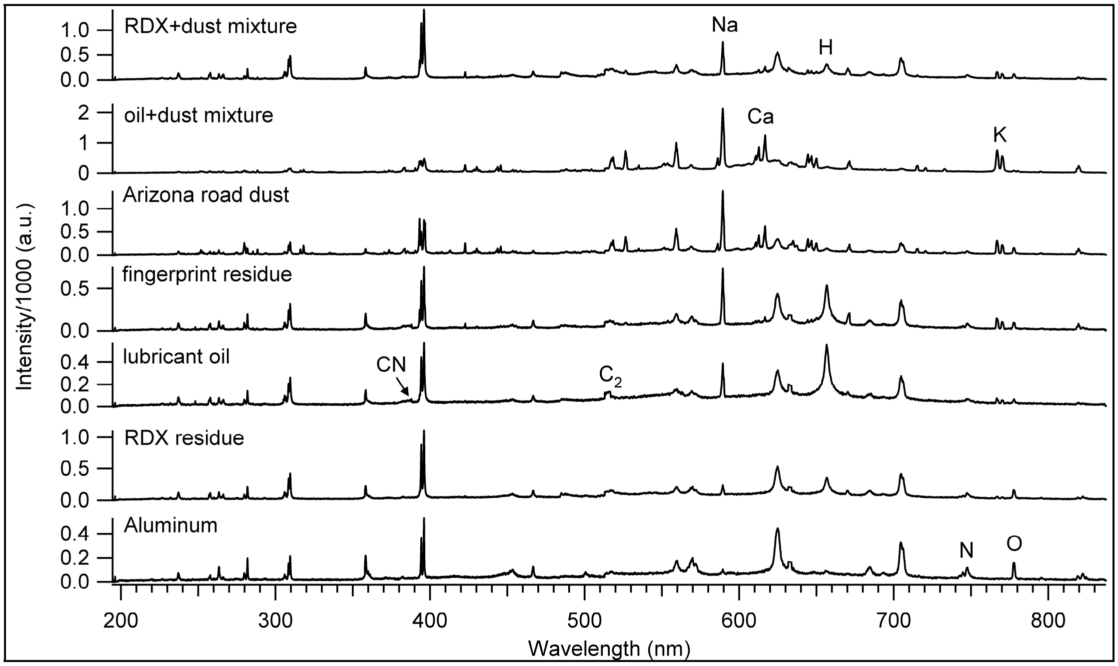

Figure 21. Single-shot spectra of RDX and interferent residues and mixtures on Al acquired at 50 m. (Strong emission lines are labeled [the C line at 247 nm does not appear].)

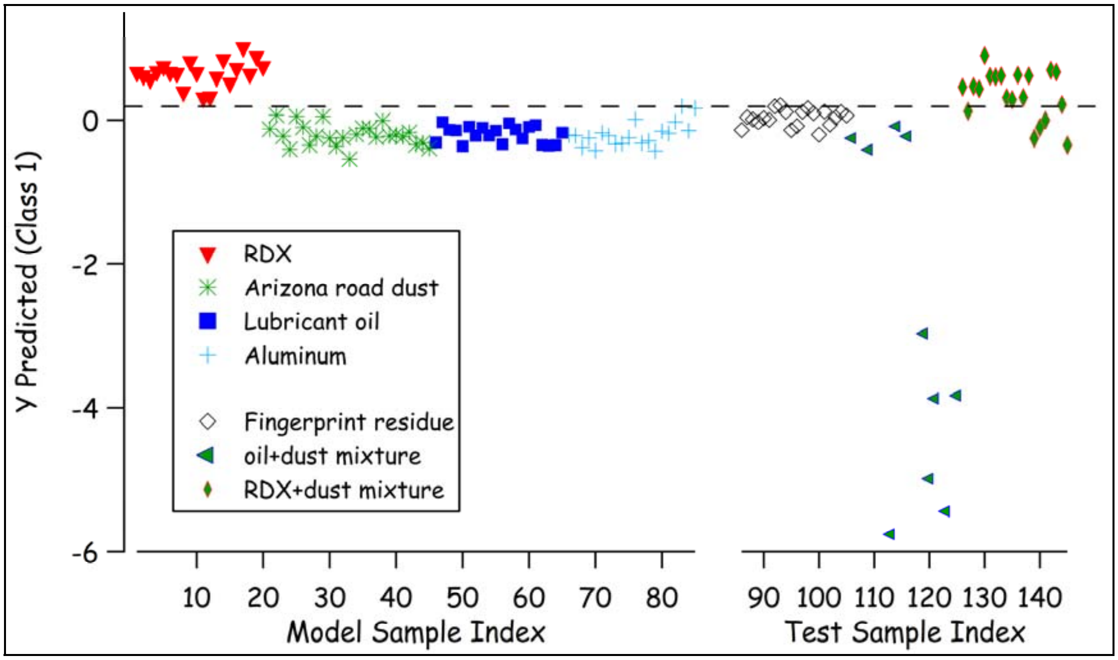

Figure 22. PLS-DA model built with spectra of RDX residue (samples 1 through 20), Arizona road dust (21 through 45), lubricant oil (46 through 65), and Al (66 through 85) acquired at 50 m. (Fingerprint residue [86-105], an oil+dust mixture [106-125] and RDX+dust mixture [126-145] were tested against the model. None of the fingerprint residues and only two of the oil+dust mixture samples [off-scale] result in false positives. Five of the RDX+dust mixture samples do not classify as explosives and possibly contained only dust in the laser-sampled region.)

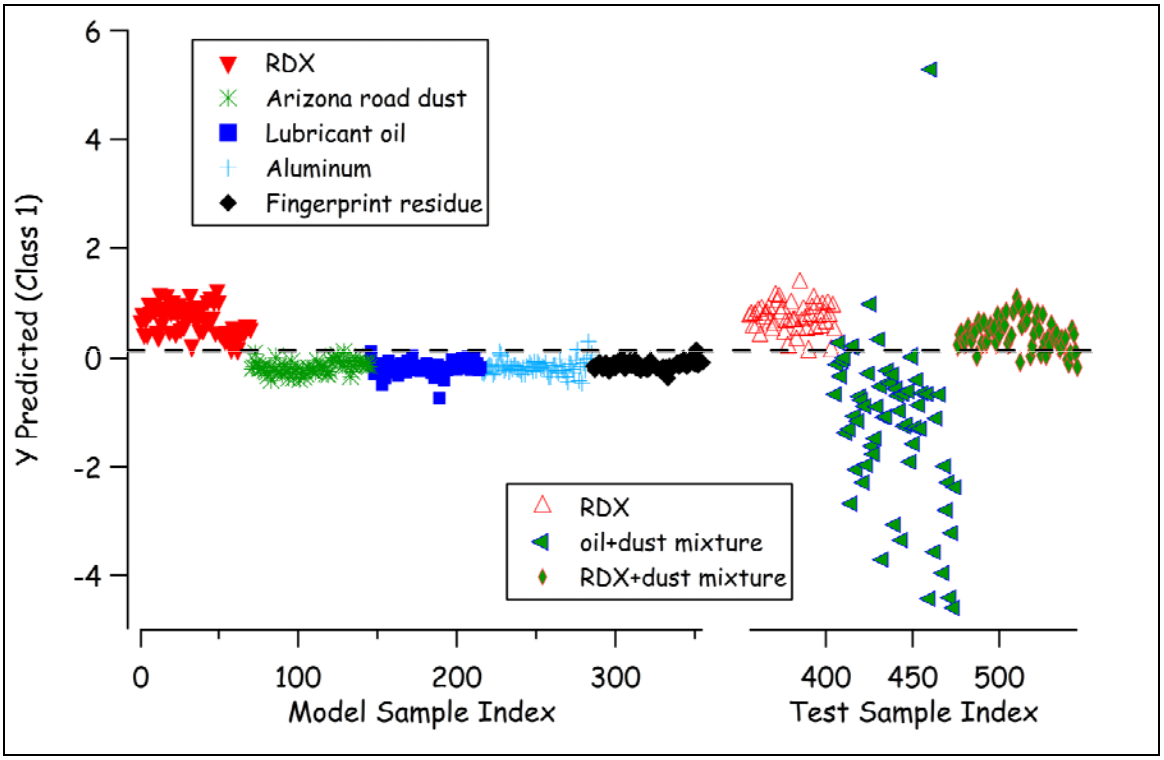

Figure 23. PLS-DA model built with spectra of RDX residue (30 m, 1-50 and 50 m, 51-70), Arizona road dust (30 m, 71-120 and 50 m, 121-145), lubricant oil (30 m, 146-195 and 50 m, 196-215), Al (30 m, samples 216-265 and 50 m, 266-285), and fingerprint residue (30 m, 286-335 and 50 m, 336-355). (RDX [30 m, 356-405], an oil+dust mixture [30 m, 406-455 and 50 m, 456-475] and RDX+dust mixture [30 m, 476-525 and 50 m, 526-545] were tested against the model. All the additional RDX residue samples were classified as explosives, as were all but nine of the RDX+dust samples [possible false negatives]. Six of the oil+dust samples resulted in false positives [8.5%].)

stand-off distances. These initial results demonstrate that it is likely that a single model can be constructed to correctly classify LIBS spectra acquired at multiple distances (so that a separate model is not needed for each possible distance).

Finally, based on the decrease in signal intensity observed in the RDX residue spectra (on an Al substrate) at the three different distances studied (20, 30, and 50 m), we estimate that the maximum effective stand-off distance of the Gen 2 ST-LIBS system is approximately 56 m (figure 24). Although we were able to obtain a LIBS spectrum of Al at 62.5 m, the strongest Al I line (396 nm) had a signal-to-noise ratio of less than 10. Spectra obtained at this distance are not likely to be analytically useful, given the limitations of the current ST-LIBS system (designed for 30 m operation). A ruggedized ST-LIBS system (with a 16-in military-specified telescope and more powerful lasers) is currently undergoing development and is expected to have an effective stand-off limit >100 m.

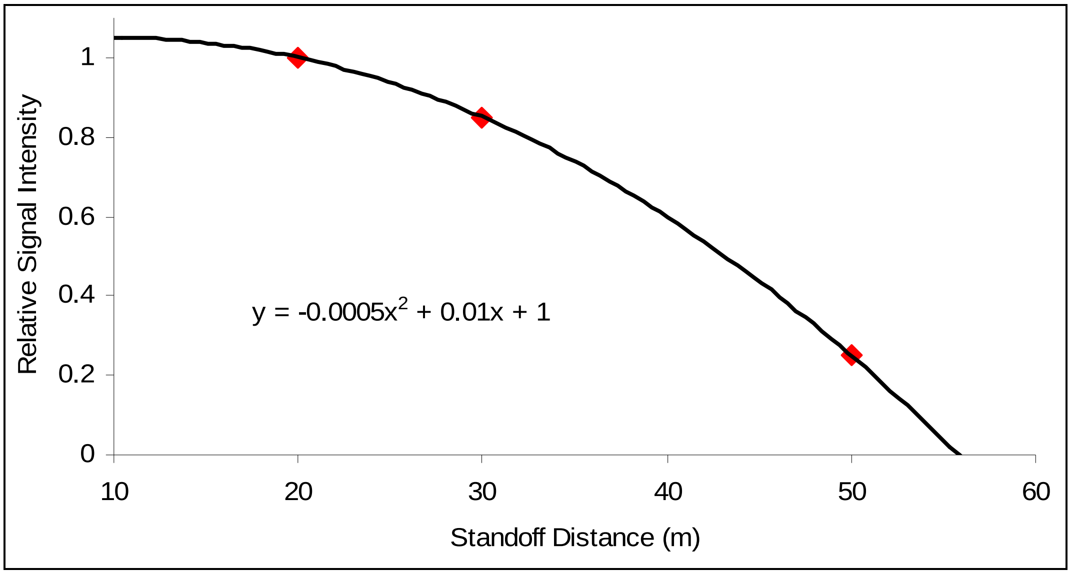

Figure 24. Estimated stand-off limit for the Gen 2 ST-LIBS system based on the signal intensities of RDX residue spectra at 20, 30, and 50 m. (A trend line connecting the points was used to estimate a maximum effective distance of 56 m.)

4. Conclusions

Recent work at ARL demonstrates the importance of eliminating the oxygen and nitrogen contribution from air for sensitive and selective LIBS detection of explosive residues (*1*). Here, we have demonstrated the detection and discrimination of explosive residues and explosive-containing mixtures as far as 50 m with a stand-off double pulse LIBS system designed to minimize the air entrainment in the LIBS plasma. Despite the typical characterization of LIBS as an elemental technique, the relative elemental intensities in the LIBS spectra are representative of the stoichiometry of the parent molecules and can be used to discriminate materials that contain the same elements. We have identified PLS-DA as an important chemometric tool for the analysis of LIBS data. Using PLS-DA, we have shown that unknown samples can be correctly classified as explosive/non-explosive even when they are not part of the library used to create the PLS-DA model.

Although stand-off LIBS is an extremely promising technology for security applications (including chemical and biological hazard detection as well as explosives detection [*6*]), some concerns need to be addressed before deployment by the military. The issue of eye safety is of practical concern when lasers are operating. While the 1064-nm radiation used in the experimental prototype ST-LIBS system (Gen 2) is not eye safe, other laser wavelengths considered somewhat eye safe can be used for LIBS. The third generation ST-LIBS system uses 1.54 μm radiation, which does not penetrate the retina. UV radiation also poses less risk for eye damage and has been used for stand-off LIBS (*7*). The appropriate design of operational

conditions can also be used to avoid unnecessary risk of eye exposure (e.g., the use of laser shut-off interlocks or removal of personnel from target areas). Finally, although LIBS is a minimally destructive technique, some minor damage does occur to the sampled surface. By using the lowest possible laser pulse energy, such damaged can be minimized. The use of microwave radiation to enhance the LIBS plasma and minimize the required laser energy is currently being investigated by ARL partners, and the initial results are extremely promising (*8*). The construction of a ruggedized ST-LIBS system capable of detecting explosive residues at >100 m is currently under way and is expected to provide an important new tool for the military in the fight against terrorism.

5. References

1. Gottfried, J. L.; De Lucia Jr. F. C.; Harmon, R. S.; Munson, C. A.; Winkel, Jr. R. J.; Miziolek, A. W. *Detection of Energetic Materials and Explosive Residues With Laser-Induced Breakdown Spectroscopy: I. Laboratory Measurements*; ARL-TR-4240; U.S. Army Research Laboratory: Aberdeen Proving Ground, MD, 2007.

2. Lopez-Moreno, C.; Palanco, S.; Laserna, J. J.; De Lucia, Jr. F. C.; Miziolek, A. W.; Rose, J.; Walters, R. A.; Whitehouse, A. I. Test of a Stand-Off Laser-Induced Breakdown Spectroscopy Sensor for The Detection of Explosive Residues on Solid Surfaces. *J. Anal. At. Spectrom.* **2006**, *21*, 55–60.

3. Gottfried, J. L.; Miziolek, A. W. ; Munson, C. A.; DeLucia, Jr. F. C.; Walters, R. Evaluation of the MP-LIBS Backpack Sensor for the Detection and Identification of Indoor Powders. *Pittcon 2006*, Orlando, FL, 12–17 March, 2006.

4. Munson, C. A.; De Lucia, Jr. F. C.; Piehler, T.; McNesby, K. L.; Miziolek, A. W. Investigation of Statistics Strategies for Improving the Discriminating Power of Laser-Induced Breakdown Spectroscopy for Chemical and Biological Warfare Agent Simulants. *Spectrochim. Acta, Part B* **2005**, *60*, 1217–1224.

5. Taschuk, M. T.; Tsui, Y. Y.; Fedosejevs, R. Detection and Mapping of Latent Fingerprints by Laser-Induced Breakdown Spectroscopy. *Appl. Spectrosc.* **2006**, *60*, 1322–1327.

6. Gottfried, J. L.; De Lucia, Jr. F. C.; Munson, C. A.; Miziolek, A. W. Double Pulse Standoff Laser-Induced Breakdown Spectroscopy (ST-LIBS) for Versatile Hazardous Materials Detection. *Spectrochim. Acta, Part B,* submitted for the LIBS2006 special issue.

7. Grönlund, R.; Lundqvist, M.; Svanberg, S. Remote Imaging Laser-Induced Breakdown Spectroscopy and Remote Cultural Heritage Ablative Cleaning. *Opt. Lett.* **2005**, *30*, 2882–2884.

8. Efthimion, P. Envimetrics Inc. Personal communication, 2007.

NO. OF COPIES	ORGANIZATION
1 (PDF ONLY)	DEFENSE TECHNICAL INFORMATION CTR DTIC OCA 8725 JOHN J KINGMAN RD STE 0944 FORT BELVOIR VA 22060-6218
1	US ARMY RSRCH DEV & ENGRG CMD SYSTEMS OF SYSTEMS INTEGRATION AMSRD SS T 6000 6TH ST STE 100 FORT BELVOIR VA 22060-5608
1	DIRECTOR US ARMY RESEARCH LAB IMNE ALC IMS 2800 POWDER MILL RD ADELPHI MD 20783-1197
3	DIRECTOR US ARMY RESEARCH LAB AMSRD ARL CI OK TL 2800 POWDER MILL RD ADELPHI MD 20783-1197
	ABERDEEN PROVING GROUND
1	DIR USARL AMSRD ARL CI OK TP (BLDG 4600)

NO. OF COPIES	ORGANIZATION
2	DIR USARL AMSRD ARL SE EO P PELLEGRINO D STRATIS-CULLUM 2800 POWDER MILL ROAD ADELPHI MD 20783-1197
3	BATTELLE EASTERN SCI & TECHNLGY CTR C W MULLINS B W JEZEK A ELLIS 1204 TECHNOLOGY DR ABERDEEN MD 21001-1228
2	NIGHT VISION AND ELECT SENSORS DIR A LAPOINTE K SHIRBANDI 10221 BURBECK RD FT BELVOIR VA 22060
1	OFC OF THE SECRETARY OF DEFENSE G A FOGG 2231 CRYSTAL DR STE 900 ARLINGTON VA 22202
1	CHEMIMAGE PATRICK J TREADO 7301 PENN AVE PITTSBURGH PA 15208
1	A3 TECHNOLOGIES LLC RICK RUSSO PO BOX 5049 WALNUT CREEK CA 94596
1	BAE SYSTEMS J F ERDMANN TECHNLGY SOLUTIONS SECTOR SYSTEMS ENGINEERING SOLUTIONS PO BOX 381 DAHLGREN VA 22448-0381
1	WHITING SCHOOL OF ENGRG MARC D DONAHUE 120 NEW ENGINEERING BLDG 3400 N CHARLES ST BALTIMORE MD 21218-2681

NO. OF COPIES	ORGANIZATION
1	IDAHO NATIONAL LAB E CESPEDES PO BOX 1625 IDAHO FALLS ID 83415-3690
1	TRANSPORTATION SECURITY LAB OFC OF RSRCH AND DEV RICHARD T LAREAU BLDG 315 TSL-200 ATLANTIC CITY INTERNATIONAL AIRPORT NJ 08405
1	NATL CENTER FOR FORENSIC SCI M E SIGMAN UNIV OF CENTRAL FLORIDA PO BOX 162367 ORLANDO FL 32816-2367
1	MATERIALS DYNAMICS GROUP D S MOORE DYNAMIC EXPERIMENTATION DIV MAILSTOP P952 LOS ALAMOS NM 87545
1	ATSE DOT CM D D DIETZ 320 MANSCEN LOOP STE 115 FT LEONARD WOOD MO 65473-8929
1	RAPID EQUIPPING FORCE J GEDDES 10236 BURBECK RD FT BELVOIR VA 22060-5852
1	US DEPT OF HOMELAND SECURITY SCI AND TECHLGY M SHEPARD WASHINGTON DC 20528
1	G GILBERT MCMR ZB T 504 SCOTT ST FT DETRICK MD 21702-5012
1	MENTIS SCIENCES J PLUMER 150 DOW ST TOWER TWO MANCHESTER NH 03101

NO. OF COPIES	ORGANIZATION
1	DEPT OF PHYSICS USMA COL R WINKEL WEST POINT NY 10996-1790
1	US ARMY RESEARCH OFC R HARMON 4300 S MIAMI BLVD DURHAM NC 27709-2211
1	ENVIMETRICS INC P EFTHIMION PO BOX 6 PLUCKEMIN NJ 07978
1	APPLIED RSRCH ASSOCIATES INC C N NORTHRUP 2672 BAYSHORE PARKWAY STE 1035 MOUNTAIN VIEW CA 94043
1	SANDIA NATIONAL LAB CONTRABAND DETECTION L THEISEN PO BOX 5800 MS0782 ALBUQUERQUE NM 87185-0782
1	PENNSYLVANIA STATE UNIV APPLIED RSRCH LAB D MERDES PO BOX 30 STATE COLLEGE PA 16804-0030
1	ENERGY RESEARCH COMPANY R DE SARO 2571-A ARTHUR KILL RD STATEN ISLAND NY 10309
1	HAMILTON SUNDSTRAND S COMBS 2771 NORTH GAREY AV POMONA CA 91767
1	AMERICAN MEASUREMENT SOLUTIONS T MARLOW 1 CORAL BELL COURT SANTA FE NM 87508

NO. OF COPIES	ORGANIZATION
	ABERDEEN PROVING GROUND
1	A W FOUNTAIN III AMSRD ECB RT D BLDG E3330/147 APG EDGEWOOD MD 21010-5424
2	USAATC CSTE DTC AT SL F C SIMPSON W BOLT BLDG 451 400 COLLERAN RD APG MD 21005-5059
1	CAMBER CORP G SCHEFFLER 5183 BLACKHAWK RD BLDG E3549 APG MD 21010-5424
18	DIR USARL AMSRD ARL WM B M ZOLTOSKI MAJ C FORD J MORRIS AMSRD ARL WM BD S PIRAINO R PESCE-RODRIGUEZ R SAUSA F DELUCIA JR A MIZIOLEK P KASTE B FORCH J GOTTFRIED M GRAMS K MCNESBY R BEYER B RICE B HOMAN J NEWBERRY C MUNSON

NO. OF COPIES	ORGANIZATION
1	A WHITEHOUSE APPLIED PHOTONICS LIMITED UNIT 8 CARLETON BUSINESS PARK SKIPTON NORTH YORKSHIRE BD23 2DE UNITED KINGDOM